European Journal of Pharmaceutical Sciences 192 (2024) 106654

Contents lists available at ScienceDirect

European Journal of Pharmaceutical Sciences

journal homepage: www.elsevier.com/locate/ejps

Development and characterization of a spray-dried inhalable ternary combination for the treatment of *Pseudomonas aeruginosa* biofilm infection in cystic fibrosis

Nasser Alhajj [a,*], Mohd Fakharul Zaman Raja Yahya [b], Niall J. O'Reilly [a,c], Helen Cathcart [a]

[a] Pharmaceutical and Molecular Biotechnology Research Centre (PMBRC), South East Technological University (SETU), Main Campus, Cork Road, Waterford X91 K0EK, Ireland
[b] Faculty of Applied Sciences, Universiti Teknologi MARA Shah Alam, 40450 Shah Alam, Selangor, Malaysia
[c] SSPC – The Science Foundation Ireland Research Centre for Pharmaceuticals, Ireland

ARTICLE INFO

Keywords:
Ciprofloxacin
Quercetin
Co-amorphous system
Cystic fibrosis
dry powder inhaler
Mucoactive agents
Biofilms *Pseudomonas aeruginosa*

ABSTRACT

Cystic fibrosis (CF) is an inherited lung disease characterised by the accumulation of thick layers of dried mucus in the lungs which serve as a nidus for chronic infection. *Pseudomonas aeruginosa* is the predominant cause of chronic lung infection in cystic fibrosis. The dense mucus coupled with biofilm formation hinder antibiotic penetration and prevent them from reaching their target. Mucoactive agents are recommended in the treatment of CF in combination with antibiotics. In spite of the extensive research in developing novel drug combinations for the treatment of lung infection in CF, to our knowledge, there is no study that combines antibiotic, antibiofilm and mucoactive agent in a single inhaled dry powder formulation. In the present study, we investigate the possibility of adding a mucoactive agent to our previously developed ciprofloxacinquercetin (antibiotic-antibiofilm) dry powder for inhalation. Three mucoactive agents, namely mannitol (MAN), N-acetyl-L-cysteine (NAC) and ambroxol hydrochloride (AMB), were investigated for this purpose. The ternary combinations were prepared via spray drying without the addition of excipients. All ternary combinations conserved or improved the antibacterial and biofilm inhibition activities of ciprofloxacin against P. aeruginosa (ATCC 10145). The addition of AMB resulted in an amorphous ternary combination (SD-CQA) with superior physical stability as indicated by DSC and nonambient XRPD. Furthermore, SD-CQA displayed better in vitro aerosolization performance (ED ~ 71 %; FPF ~ 49 %) compared to formulations containing MAN and NAC (ED ~ 64 % and 44 %; FPF ~ 44 % and 29 %, respectively). In conclusion, a ternary drug combination powder with suitable aerosolization, physical stability and antibacterial/antibiofilm properties was prepared by a single spray drying step.

1. Introduction

Pseudomonas aeruginosa is the main contributor pathogen to the morbidity and mortality in adult cystic fibrosis (CF) patients (Bernardy et al., 2020). *P. aeruginosa* is one of the most critical antibiotic-resistant pathogens according to the World Health Organization (WHO) (Mancuso et al., 2021); it has a multiple virulence factors including biofilm formation (Qin et al., 2022) which is the most significant hallmark of *P. aeruginosa*. In chronically infected CF patients, *P. aeruginosa* encapsulates itself in a self-produced extracellular polymeric substances (EPS; biofilms) which enables the bacterium to survive under harsh conditions such as nutrient deficiency and antibiotics (Liao et al., 2022). The treatment of *P. aeruginosa* lung infection becomes even more challenging in CF patients due to the hypersecretion of dehydrated airway mucus which impairs the mucociliary clearance system (Hill et al., 2018).

Ciprofloxacin is a commonly used antibiotic in the treatment of lung infections and is one of the most effective antibiotics against *P. aeruginosa* (Thai et al., 2021). Ciprofloxacin is a concentration-dependent fluoroquinolone antibiotic whose efficacy depends on delivering sufficient amounts of ciprofloxacin to the site of action. However, low concentrations of ciprofloxacin promotes *P. aeruginosa* resistance against ciprofloxacin and cross-resistance to other antibiotics such as beta-lactams (Ahmed et al., 2020). Unfortunately, systemic administration of a high dose of ciprofloxacin can result in a severe adverse effects; thus developing inhaled ciprofloxacin for pulmonary targeted delivery with minimum systemic exposure has a

* Corresponding author.
E-mail address: nasser.al-hajj@postgrad.wit.ie (N. Alhajj).

https://doi.org/10.1016/j.ejps.2023.106654
Received 4 June 2023; Received in revised form 23 November 2023; Accepted 24 November 2023
Available online 25 November 2023

Table 1
The mass content and molar ratio of the solid ingredients in the feedstocks

Formulation	CIP (mg)	QUE (mg)	Mucoactive Agent			CIP:QUE:Mucoactive (molar ratio)	Solvent
			MAN (mg)	NAC (mg)	AMB (mg)		
SD-CIP	3000	-	-	-	-	1:0:0	Ethanol 75 % v/v
SD-QUE	-	3000	-	-	-	0:1:0	Ethanol 75 % v/v
SD-CQ	1682.21	1317.79	-	-	-	1:1:0	Ethanol 75 % v/v
SD-CQM	1330.07	1041.93	628.00	-	-	1:1:1	Ethanol 75 % v/v
SD-CQN	1359.72	1065.16	-	575.12	-	1:1:1	Ethanol 75 % v/v
SD-CQA	1292.76	1012.71	-	-	694.53	1:1:0.5	Ethanol 75% v/v

Note: SD means spray-dried; CIP and QUE mean ciprofloxacin and quercetin; CQ, CQM, CQN and CQA mean ciprofloxacin-quercetin, ciprofloxacin-quercetin-mannitol, ciprofloxacin-quercetin-N-acetylcysteine, ciprofloxacin-quercetin-ambroxol combinations, respectively.

promising role in the treatment of lung infections (Alhajj et al., 2021).

Quercetin is a flavonol with a promising role in the treatment of CF. It has the ability to activate the mucociliary clearance system via stimulating chloride ion secretion and improving ciliary beat frequency (Asano et al., 2009; Zhang et al., 2011). Quercetin also shows promising activity against *P. aeruginosa*. It increases the susceptibility of *P. aeruginosa* to antibiotics via damaging the bacterial membrane integrity and wall ultrastructure (Wang et al., 2018). Quercetin also inhibits several *P. aeruginosa* virulence factors such as quorum sensation and biofilm formation (Ouyang et al., 2016; Paczkowski et al., 2017; Vasavi et al., 2016; Vipin et al., 2019).

Mucoactive agents are used in CF therapy to reduce the viscosity of mucus and improve the clearance of sputum. Mucoactive agents are usually combined with antibiotics in the treatment of CF lung infection in order to improve the penetration of antibiotics through mucus layers and hence boost the antimicrobial outcome (Brunaugh et al., 2021).

In our previous work, we developed a physically stable, fixed-dose, inhalable, ciprofloxacin-quercetin dry powder via spray drying without the use of excipients (Alhajj et al., 2023, 2022). We found that co-spray drying ciprofloxacin and quercetin at a 1:1 molar ratio yielded the most promising dry powder with excellent physical stability and good aerosolization properties. The present work investigates the possibility of adding a mucoactive agent to our previously developed formulation to form ternary, fixed-dose combinations composed of ciprofloxacin (antibiotic), quercetin (antibiofilm) and a mucoactive agent. The aim is to develop a formulation that delivers a high dose of ciprofloxacin directly to the lung in combination with a mucoactive and an antibiofilm agent in order to facilitate its penetration through the mucus layers and biofilm towards the bacterium.

To this end, three mucoactive agents with well-established clinical use in CF therapy (Henke and Ratjen, 2007; Ratjen et al., 1985; Varelogianni et al., 2013) were selected for this investigation. The selected mucoactive agents are mannitol (MAN; a hyperosmotic agent), N-acetyl-L-cysteine (NAC; a mucolytic agent) and ambroxol hydrochloride (AMB; a mucokinetic agent) (Tarrant et al., 2019). MAN, NAC and AMB vary in their molecular weights, hydrophilic/hydrophobic properties (logP values are -3.7, -0.71 and +2.65, respectively) and water/ethanol solubility. Thus, they are expected to exhibit different behaviour during the spray drying process and subsequently different influences on the physicochemical characteristics of the dried particles.

In this work, dry powders of ciprofloxacin, quercetin, ciprofloxacin-quercetin binary combination and ciprofloxacin-quercetin-mucoactive ternary combinations were prepared via spray drying. The solid state and the moisture sorption behaviour of the powders was investigated as well as other powder properties such as particle size, morphology, density, cohesion, and residual moisture content. The dissolution profiles and aerodynamic performance of ciprofloxacin and quercetin were investigated from their unary, binary and ternary formulations. Finally, the antibacterial and antibiofilm activities of the antibiotic and its combinations were studied.

2. Method

2.1. Materials

Ciprofloxacin hydrochloride monohydrate (CIP), anhydrous quercetin (QUE) and ambroxol hydrochloride (AMB) were obtained from Carbosynth Limited (Berkshire, U.K.). N-acetyl-L-cysteine was obtained from ThermoFisher (Kandel, Germany) and mannitol from Fisher Scientific (Loughborough, UK). Buffered Saline Tablets (Sigma-Aldrich Ireland Limited, Arklow, Ireland) were used to prepare phosphate buffer solution (PBS) pH 7.4. All other solvents were of analytical grade.

2.2. Preparation of spray dried powders

Spray-dried powders were prepared using a Pro-CepT 4M8-TriX spray dryer (Zelzate, Belgium). Separate solutions were prepared by dissolving CIP and QUE in water and ethanol, respectively. The CIP solution was then added gradually to the QUE solution under continuous stirring. For the ternary feedstock solutions, MAN and NAC were dissolved in the CIP aqueous solution while AMB was dissolved in the QUE ethanolic solution. The aqueous solutions were added gradually to the ethanol solution under continuous stirring. The total solid content of the feedstocks was 3000 mg dissolved in 300 ml of co-solvent (water: ethanol 25:75 v/v) resulting in a total solid concentration of 1 % w/v. The compositions of the different formulations are presented in Table 1.

The spray drying was performed under the following processing condition: nozzle orifice diameter 0.4 mm, air flow 0.3 m^3/min, differential pressure over cyclone 50 mbar, solution flow rate 4.5 g/min (100 % pump speed), atomizing air flow rate 8.5 L/min, and inlet temperature 100°C. Screw-capped glass scintillation vials were used for collecting the dried powder which were then stored in a desiccator over silica gel at room temperature until further use. The process yield was calculated from the total solid mass of the sprayed feedstock and the mass of the spray-dried powder recovered.

2.3. Particle morphology

The morphology of the spray-dried particles was investigated using a scanning electron microscope (SEM). A TM4000 SEM (Hitachi High-Technologies, UK) was used to capture particle images at an accelerating voltage of 10 kV. The spray-dried powders were fixed onto a metal stub using double-sided carbon adhesive tape and then sputter coated with a thin layer of gold (approximately 20 nm) under vacuum using an Emitech K550 sputtering instrument (Emitech, UK).

2.4. Particle size distribution

The particle size distribution of the powders was determined using laser diffraction. A Scirocco 2000 powder dispersion unit attached to a Mastersizer 2000 laser diffraction instrument (Malvern Instruments, UK) was used to take the measurements at a dispersive air pressure of 1 bar and a vibration rate between 25 and 50 % which achieved an obscuration of between 0.5 and 6 %. A refractive index of 1.572 and an

absorption of 0.01 were used for SD-CIP powder while a refractive index of 1.823 and an absorption of 0.10 were used for SD-QUE and the spray-dried combinations.

The particle size was expressed as volume based geometric diameters $D_{(v,10)}$, $D_{(v,50)}$, and $D_{(v,90)}$, and the size distribution was expressed as the span values:

$$\text{Span value} = \frac{D(v,90) - D(v,10)}{D(v,50)} \quad \text{(Eq. (1))}$$

2.5. Powder density

The bulk (ρ_b) and tapped (ρ_t) densities were measured using a 1 ml tuberculin syringe (de Castro et al., 2020). Briefly, powder was poured under gravity to fill the syringe to 0.5 ml mark (bulk volume) and the mass of the powder was taken. Then the syringe was tapped vertically on a level bench-top surface from a height of 5 cm until no further reduction in the volume was observed (tapped volume). The bulk (ρ_b) and tapped (ρ_t) densities were calculated by dividing the powder mass by the corresponding volume. Carr's index was calculated from the bulk and tapped densities using the following equations:

$$Carr's\ index\ (100) = \left(1 - \left(\frac{b\rho}{t\rho}\right)\right) \times 100 \quad \text{(Eq. (2))}$$

2.6. Powder cohesion

The cohesion (C) of the powders was determined using an FT4 powder rheometer (Freeman Technology Ltd., UK). A 1 ml shear cell module was filled with 500 mg powder and a vented piston was used to condition the sample under a normal stress of 9 kPa. A shear head was used to measured the shear stress under normal stresses of 3, 4, 5, 6 and 7 kPa. The yield loci, under a given normal stress, is the maximum shear stress that the bed can support. Cohesion is the yield loci at zero normal stress which is calculated as (Mangal et al., 2019b):

$$C = \tau - \sigma \tan\eta \quad \text{(Eq. (3))}$$

where τ is the shear stress, σ is the normal stress and η is the angle of friction.

2.7. Residual moisture content

The residual moisture content of the powders was measured using a Q50 TGA Thermogravimetric Analyzer (TA instruments, UK). Between 5 and 10 mg powder was loaded onto a platinum pan and heated at a rate of 10°C min^{-1} from 25°C to 500°C. The measurement was performed under a nitrogen atmosphere with a purge gas flow rate of 50 ml min^{-1}. The residual moisture content of the samples was calculated based on the percentage of weight loss with increasing temperature between 25°C and 100°C using TRIOS software (TA instruments, UK).

2.8. Dynamic vapour sorption (DVS)

The moisture sorption behaviour of the powders was investigated using dynamic vapor sorption (DVS-Intrinsic, Surface Measurement Systems Ltd., UK). A mass of 10 to 15 mg was initially equilibrated at 0 % relative humidity (RH) until a steady dry reference mass was recorded. The RH was changed from 0 to 90 % and the reverse for desorption in 10 % RH steps at 25°C. The end of each stage was taken as the point where dm/dt was $\leq$ 0.002 % mg min^{-1} over 10 min.

2.9. Differential scanning calorimetry (DSC)

The thermal properties of the powders were assessed using a differential scanning calorimeter Q2000 DSC (TA Instruments, UK) calibrated using an indium calibration standard (TA Instruments, UK). A sample of 3 to 5 mg was crimp-sealed in Tzero™ Hermetic sample pans with three pin holes. The sample was scanned between 0°C to 400°C at a rate of 10°C min^{-1} under a nitrogen gas flow of 50 ml min^{-1}. In order to aid the detection of the glass transition temperature (Tg), powders were subjected to modulated differential scanning calorimetry (mDSC) (Karagianni et al., 2018). A sample prepared as above was scanned between 0 and 400°C at a heating rate of 2°C min^{-1} with a modulation amplitude of ±1°C and a modulation period of 60 s. TRIOS software (TA instruments, UK) was used for analysing the thermograms.

2.10. X-ray powder diffraction (XRPD)

The crystallinity of the powders was determined using a Bragg-Brentano diffractometer (D8 Advance, Bruker). Samples were irradiated with monochromatized CuKα radiation (1.5406 Å) and scanned between 5 and 50° (2θ). The patterns were recorded under the following conditions: voltage, 40 kV; current, 40 mA; constant, 1 s; angular step 0.02°. Measurements under ambient condition were conducted using a flip-stick stage and an anti-scatter screen. Environmental XRD was performed using an Anton-Paar (CHC plus+) non-ambient stage to study the evolution of phases at different humidities or temperature. To investigate the influence of humidity, the RH was increased from 0 to 90 % in 10 % RH steps at 25°C; the samples were scanned at each RH point after a delay of 3 h, in accordance with the DVS isotherms. To investigate the effect of temperature, the powders were heated with a heating ramp rate of 2°C min^{-1} and the measurements were taken at predetermined temperature points based on their corresponding mDSC curves.

2.11. Fourier transform infrared (FTIR) spectroscopy

Infrared spectra were recorded using an FTIR Spectrometer (Varian 660-IR, Australia) between 400 and 4000 cm^{-1} at a resolution of 4 cm^{-1}. The sample was mixed with dry KBr at a mass ratio of 2:98, respectively, in an agate mortar. The blend was pressed into a self-supporting disc at 3 tons for 3 min using a pellet die (diameter 13 mm) and a hydraulic pellet press (Specac Ltd., UK).

2.12. X-ray photoelectron spectroscopy (XPS)

The elemental composition at the particle surface of the spray-dried single drug and drug combination powders was determined using XPS. A Kratos AXIS ULTRA spectrometer (Kratos Analytical, Manchester, UK) connected to a monochromatized AlKα X-ray (1486.58 eV) source at a power of 300 W (20 mA, 15 kV) was used to collect the spectra. Each of the powder samples were loaded into shallow well sample holders, and the spectra were collected using an analysis area of 1 mm^2. The charge of the irradiated samples was neutralized using an electron flood gun combined with a magnetic immersion lens. A reference binding energy (BE) of 285.0 eV for C1s was used for the correction of any remaining offsets due to charge neutralization. The low-resolution survey spectra were collected at a constant analyser pass energy of 160 eV and subsequently narrow high-resolution spectra were acquired for the individual peaks at 20 eV with 0.05 eV steps. The data were processed using Casa XPS software. Peak areas were converted to atomic concentrations and normalized to a total concentration of 100 %.

2.13. In vitro aerosolization by next generation impactor (NGI)

The aerosolization performance of the powders was determined using a next generation impactor (NGI; Copley Scientific Ltd., UK) equipped with Copley HCP5 vacuum pump and Copley TPK 2000 critical flow controller. A Copley DFM 2000 electronic digital flow meter was used to verify the air flow rate. All NGI cups were coated with 1 ml of a Span 80:Methanol solution (2:98, v/v, respectively) and left untill fully dried before running the test. A powder sample of 20 mg was filled into a size 3 hard gelatine capsule for DPI (Capsugel, Germany) and

inserted into a Cyclohaler® inhaler device. The Cyclohaler® with a punctured capsule was connected into a stainless steel induction port (IP) through a mouthpiece (MP) adaptor. The dispersion was carried out at a flow rate of 60 L/min for 4 s (Srichana et al., 1998). At this flow rate, the cut-off diameters of the individual stages from 1 to 7 were 8.06, 4.46, 2.82, 1.66, 0.94, 0.55, 0.34 μm, respectively. After actuation, the powders which were deposited on the MP, IP, all NGI stages and micro-orifice collector (MOC) in addition to the powders retained in the capsule shell and the inhaler device were collected, dissolved in mobile phase and samples were analysed using HPLC.

The aerodynamic parameters were calculated as follow: the total recovered dose (RD) was the sum of the drug collected from all parts (i.e. capsule shell, inhaler device, MP, IP, all NGI stages and MOC); the recovered dose percentage (RD%) is the RD expressed as percentage of the amount of drug introduced into the capsule; the emitted dose (ED) was the subtraction of the retained powders in capsule shell and inhaler device from the total recovered dose; the emitted dose (ED%) is the ED expressed as percentage of the RD; the fine particle dose (FPD) was the sum of the powders deposited from stage 3 to MOC; the fine particle fraction (FPF) is the FPD expressed as a fraction of the RD. The mass median aerodynamic diameter (MMAD) and the geometric standard deviation (GSD) were obtained by interpolation from the aerodynamic particle size distribution plot.

2.14. In-vitro dissolution study

The dissolution profiles of as-received ciprofloxacin, quercetin and the spray-dried formulations were measured under sink conditions in phosphate buffer saline (PBS) with 0.1 % w/v tween 80 at pH 7.4 and 37°C. Accurately weighed quantities of each sample (equivalent to 2.5 mg ciprofloxacin and 1.96 mg quercetin) were added to 45 ml of dissolution medium maintained at 37°C and shaken at 100 rpm in an orbital shaker-Incubator Grant bio ES-20 (Grant Instruments, UK). A sample of 2 ml was taken at 5, 10, 15, 30, 60, 90, 120, and 240 min time intervals and immediately replaced by 2 ml fresh medium. The percentage of drug released was calculated based on the drug content of the dry powder. Each experiment was carried out in triplicate and the results averaged. Considering that there is no regulatory guideline on the formula of lung simulated fluid, PBS has been widely used as a simple dissolution media for inhalation formulations which reflects the buffering capability of the lung fluid (Mangal et al., 2019a; Eedara et al., 2022). Tween 80 has been used in different dissolution media, including media for pulmonary formulations, to maintain the sink conditions of drugs with very poor water solubility (Bhagwat et al., 2017; Son et al., 2010).

2.15. In vitro antibacterial activity

The minimum inhibitory concentration (MIC) of as-received CIP and the spray-dried formulations against *P. aeruginosa* (ATCC 10145) was determined by the broth microdilution method in accordance with the Clinical and Laboratory Standards Institute (CLSI) guidelines (Wayne, 2010). Both CIP and the formulations were initially dissolved in DMSO and subsequently diluted using Luria-Bertani medium (LB) to the desired ciprofloxacin concentrations. Two-fold dilutions were prepared, with final ciprofloxacin concentrations of 0.125, 0.25, 0.5, 1, 2, 4, 8 and 16 μg/mL and DMSO concentration of 2 %. To obtain the treated group, 100 μL of the treatment sample and 100 μL of the overnight bacterial culture suspension (optical density $OD_{600} = 0.05$) were mixed in 96-well plates (Corning Incorporated, Corning, USA) which resulted in a final ciprofloxacin concentration of 0.0625, 0.125, 0.25, 0.5, 1, 2, 4, and 8 μg/mL with 1 % DMSO. Wells containing bacteria treated with only 1 % DMSO served as negative control and wells containing uninoculated media served as positive control. Treated and non-treated bacteria were incubated for 24 h at 37 °C. The ODs were measured using an Epoch microplate reader (BioTek Instruments Inc., USA). The MIC was defined as the lowest concentration that reduced OD_{600} by ≥ 95 % (Lababidi et al., 2019).

In addition, the bacterial inhibition potential of CIP and the spray-dried combinations was determined according to the method reported by Lababidi et al. (2020). Briefly, an overnight culture of *P. aeruginosa* (ATCC 10145) in the exponential growth phase was diluted to a final OD_{600} of 0.2 in LB broth. 100 μL of bacterial suspension was added into 96-well plates and 100 μL of the treatment sample was added resulting in ciprofloxacin concentration range as the above-mentioned protocol. Positive and negative controls and the treated culture were incubated for 24 h at 37 °C. OD_{600} was measured using an Epoch microplate reader (BioTek Instruments Inc., USA). Bacterial inhibition was calculated as:

$$\text{Bacterial inhibition } (\%) = \left(1 - \frac{OD_{600}\ treated\ sample}{OD_{600}\ \text{untreated control}}\right) \times 100 \quad \text{(Eq. (4))}$$

2.16. In vitro antibiofilm activity

2.16.1. Inhibition of biofilm formation

Determination of the effects of as-received CIP and the spray-dried formulations on the formation of *P. aeruginosa* (ATCC 10145) biofilm was performed using the crystal violet (CV) assay according to procedures reported by Merritt et al. (2011) with slight modifications. 100 μL of overnight bacterial culture ($OD_{600} = 0.6$) was added to a 96-well plate (Corning Incorporated, Corning, USA). 100 μL solution of CIP and the spray-dried combinations in LB (DMSO 2 %) were add to the wells to give 4 concentrations of ciprofloxacin for each sample (i.e. ½ MIC, 1 MIC, 2 MIC and 4 MIC). Wells containing bacteria treated with only 1 % DMSO served as a negative control and wells containing uninoculated media served as the positive control. After 24 h incubation at 37 °C, the growth medium containing floating cells was discarded from the plate. The wells were rinsed twice with sterile distilled water and then stained with 200 μL of CV 0.1 % (w/v) and kept for 30 min at room temperature. CV was removed and the wells were rinsed twice with sterile distilled water to remove excess CV. Stained biofilms were dissolved in absolute ethanol and the biomass was measured at OD_{590} using an Epoch microplate reader (BioTek Instruments Inc., USA). The percentages of biofilm formation were expressed in relation to the untreated control. Each assay was carried out in triplicate.

$$\text{Biofilm formation } (\%) = \frac{treated\ sample}{\text{untreated control}} \times 100 \quad \text{(Eq. (5))}$$

2.16.2. Disruption of pre-formed biofilms

P. aeruginosa (ATCC 10145) biofilm was formed according to the method reported by Chang et al. (2019), with slight modification. Briefly, ATCC 10145 strain was grown in LB medium for 24 h at 37°C. Then 100 μL of overnight bacterial culture ($OD_{600} = 0.6$) was added to 100 μL of LB into 96-well plates (Corning Incorporated, Corning, USA) and incubated at 37°C for 48 h. Biofilm was washed with sterile distilled water and then treated with 200 μL of the treatments at ½ MIC, 1 MIC, 2 MIC and 4 MIC of ciprofloxacin and incubated at 37°C for 24 h. The biofilm was washed twice using sterile distilled water. Biofilm biomass was measured by crystal violet as per above protocol. Three replicates were performed for each condition. The percentage of the biofilm remaining after the disruption test was expressed in relation to the untreated control according to Eq. (5).

2.17. Quantification by HPLC

The quantitative determination of ciprofloxacin and quercetin in the powders was conducted using an isocratic reverse-phase HPLC system (Agilent Technologies series 1200 HPLC consisting of an auto-sampler, binary pump, column oven, and DAD detector) equipped with a Kinetex-C18 column (150 mm × 4.6 mm, internal diameter 5 μm,

Table 2
Yield, residual moisture content, volume based geometric diameters and powder properties of spray-dried formulations (mean ± SD, n = 3).

Formulations	Yield (%)	RMC (%)	$D_{(v,10)}$(μm)	$D_{(v,50)}$(μm)	$D_{(v,90)}$(μm)	ρ_b (g/ml)	ρ_t (g/ml)	Carr's Index(%)	Cohesion (kPa)
SD-CIP	70.8	4.91±0.02	1.09 ± 0.11	4.24 ± 0.14	13.19 ± 0.7	0.20±0.01	0.47±0.05	57.12±2.56	4.01 ± 0.37
SD-QUE	63.6	3.98±0.16	1.07 ± 0.07	2.48 ± 0.08	5.30 ± 0.18	0.25±0.01	0.57±0.04	55.19±3.03	3.49 ± 0.15
SD-CQ	73.9	2.90±0.16	0.88 ± 0.03	2.34 ± 0.02	5.10 ± 0.18	0.31±0.02	0.64±0.04	52.00±3.46	3.35 ± 0.11
SD-CQM	74.5	2.89±0.33	0.87 ± 0.03	2.10 ± 0.02	4.61 ± 0.16	0.36±0.03	0.65±0.05	44.67±2.31	3.20 ± 0.13
SD-CQN	77.5	2.31±0.21	0.75 ± 0.01	1.94 ± 0.02	4.01 ± 0.33	0.40±0.02	0.82±0.06	51.33±2.31	3.32 ± 0.03
SD-CQA	77.7	3.47±0.16	1.09 ± 0.04	2.46 ± 0.09	5.31 ± 0.52	0.36±0	0.57±0.04	36.67±5.03	2.77 ± 0.07

Note: RMC means residual moisture content; $D_{(v,10)}$, $D_{(v,50)}$ and $D_{(v,90)}$ mean volume based geometric diameters at 10 %, 50 % and 90 %, respectively; ρ_b and ρ_t mean bulk density and tapped density, respectively; SD means spray-dried; CIP and QUE mean ciprofloxacin and quercetin; CQ, CQM, CQN and CQA mean ciprofloxacin-quercetin, ciprofloxacin-quercetin-mannitol, ciprofloxacin-quercetin-N-acetylcysteine, ciprofloxacin-quercetin-ambroxol combinations, respectively.

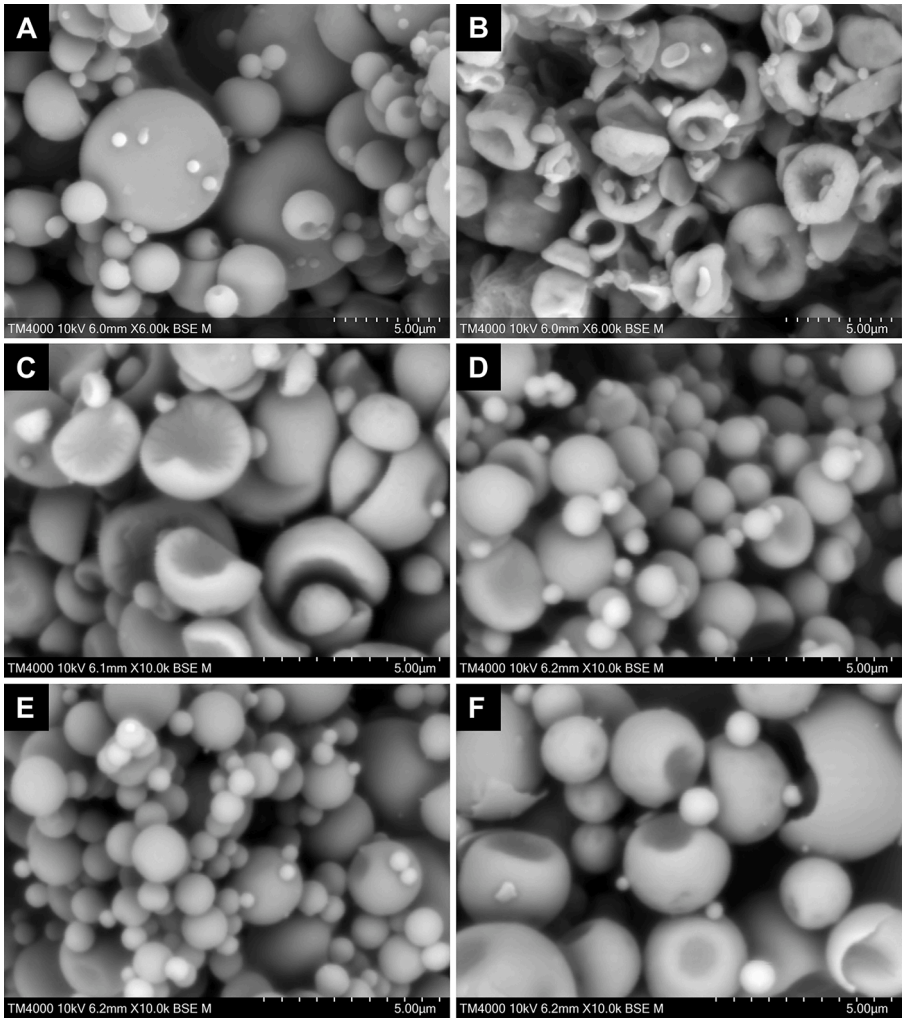

Fig. 1. SEM images of: A) SD-CIP; B) SD-QUE; C) SD-CQ; D) SD-CQM; E) SD-CQN; F) SD-CQA; SD means spray-dried; CIP and QUE mean ciprofloxacin and quercetin; CQ, CQM, CQN and CQA mean ciprofloxacin-quercetin, ciprofloxacin-quercetin-mannitol, ciprofloxacin-quercetin-N-acetylcysteine, ciprofloxacin-quercetin-ambroxol combinations, respectively.

Phenomenex, UK). The mobile phase consisted of water and acetonitrile (45:55, %v/v), adjusted to pH 2.1 by adding 0.1 % v/v trifluoroacetic acid (TFA). The injection volume was 20 μl and the flow rate was 1 ml/min with a run time of 5 min at 35°C. The wavelength for detection was 258 nm. The calibration curves were linear ($R^2 = 0.999$) over the concentration range of 0.5–96 μg/ml for each drug with a retention time of 1.5 and 2.1 min for ciprofloxacin and quercetin, respectively.

2.18. Statistical analysis

Minitab (Minitab Inc., Version 20, State College, PA, USA) was used to conduct the statistical analysis. One-way analysis of variance (ANOVA) with post hoc Tukey test was carried out to compare differences between groups. Dunnett's multiple comparison test was used in the *in vitro* antibacterial and antibiofilm studies to compare the spray-dried combinations to CIP.

3. Result and discussion

The process yield of the spray dried powders ranged between 63.6 and 77.7 % (Table 2).

The lowest process yield was of SD-QUE followed by SD-CIP. The

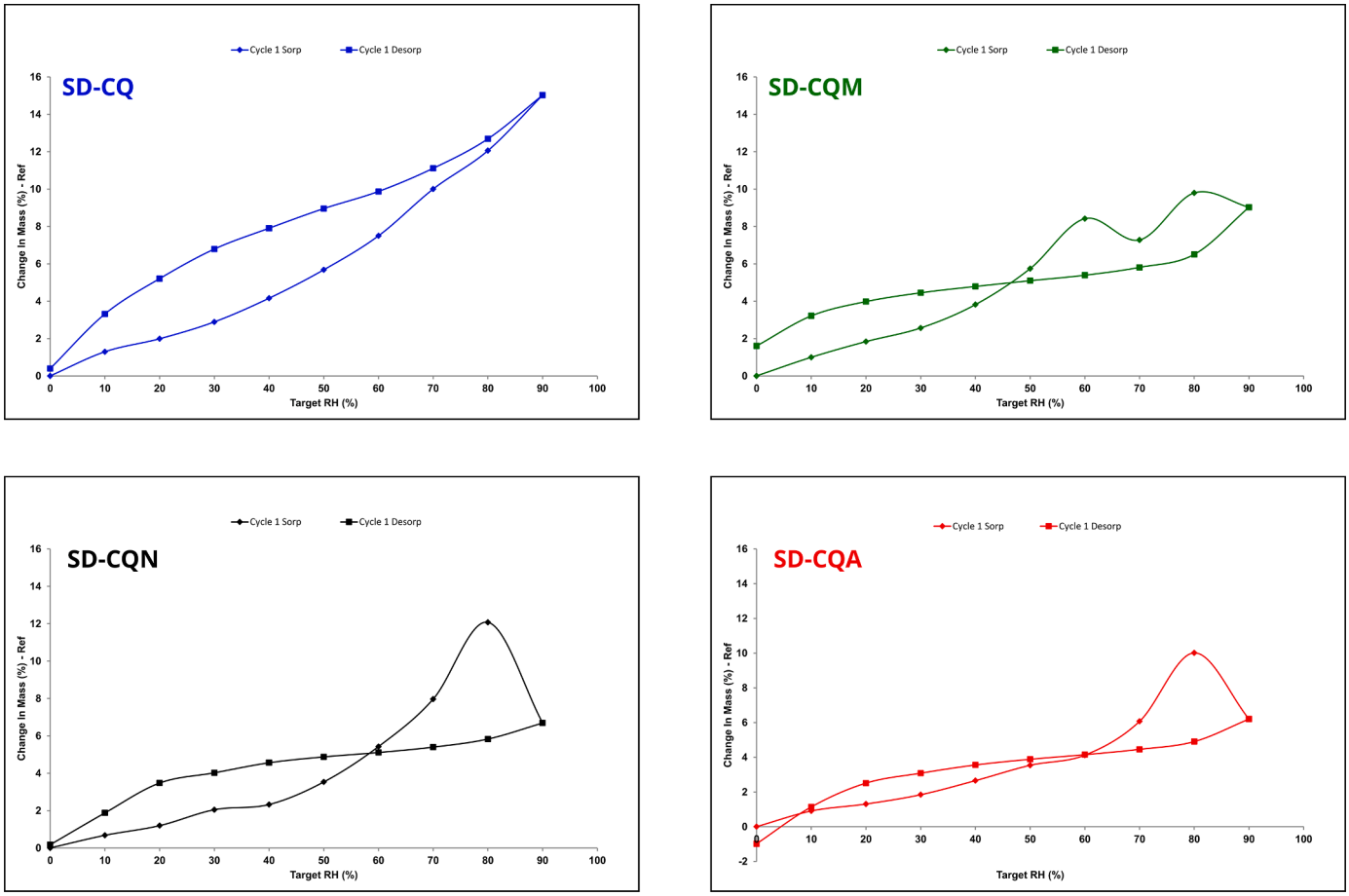

Fig. 2. Moisture sorption isotherms of spray-dried powders; SD means spray-dried; CIP and QUE mean ciprofloxacin and quercetin; CQ, CQM, CQN and CQA mean ciprofloxacin-quercetin, ciprofloxacin-quercetin-mannitol, ciprofloxacin-quercetin-N-acetylcysteine, ciprofloxacin-quercetin-ambroxol combinations, respectively. Triangles are for the sorption branch and squares for the desorption branch of the isotherms.

comparatively low yield of these formulations was caused by the powder depositing on the walls of the spray dryer rather than reaching the collector as discussed in our previous work (Alhajj et al., 2022). Table 2 shows that co-spray drying CIP and QUE together in the binary and ternary systems improved the process yield compared to spray-drying CIP or QUE individually. The average content of CIP and QUE in the spray-dried combinations was calculated based on their theoretical content and found to be between 94 and 105 % (Table S1).

3.1. Size and morphology

Apart from SD-CIP, all spray dried powders had favourable particle size distributions for pulmonary delivery with $D_{(v,50)}$ and $D_{(v,90)}$ of < 2.5 μm and < 5.5 μm respectively. Among the spray-dried combinations, SD-CQM and SD-CQN both had significantly lower $D_{(v,50)}$ than other combinations ($p < 0.05$ and $p < 0.001$, respectively). It is noteworthy that these two formulations include small hydrophilic mucoactive molecules i.e. MAN and NAC, respectively, which are expected to have a higher diffusion rate during the drying process and hence a reduced Péclet number resulting in lower particle sizes compared to SD-CQ and SD-CQA.

Fig. 1. presents SEM images of the spray-dried formulations. SD-CIP particles were spherical in shape with smooth surfaces while SD-QUE particles were collapsed spheres which can be attributed due to the hydrophobic nature of quercetin (Alhajj et al., 2022). The binary combination SD-CQ particles displayed a hemispherical shape with smooth surfaces. The addition of a hydrophobic third agent (in SD-CQA) produced spherical particles with occasional wall depressions while the addition of a hydrophilic third drug (SD-CQM or SD-CQN) resulted in the formation of particles with more perfect sphericity.

3.2. Residual moisture content

The residual moisture content of the spray-dried powders was calculated as the weight loss of the sample when heated from room temperature to 100°C using TGA (Fig. S1). All spray-dried powders had a residual moisture content below 5 %. The residual moisture content of SD-CQ was lower than the single drug powders at 2.90 %. The ternary combinations, showed no significant difference in their residual moisture content compared to the binary formulation. In conclusion, the residual moisture content of SD-CIP was significantly reduced ($p < 0.05$) when co-spray-dried with quercetin alone or with the addition of a third ingredient.

3.3. Dynamic vapour sorption (DVS)

The moisture sorption isotherms of the spray-dried combination powders are presented in Fig. 2. For individually spray-dried drugs (Fig. S2), the moisture sorption isotherms of SD-CIP and SD-QUE showed a significant mass increase due to their amorphous phase transition to a crystalline form (Alhajj et al., 2022).

It is clear that the ternary combinations exhibited different sorption isotherm behaviour compared to SD-CQ. The SD-CQM exhibited two crystallization events at 60 and 80 % RH. The change during the sorption cycle was irreversible since the desorption isotherm did not return to its initial value, showing a mass increase of ~2 % at the end of the

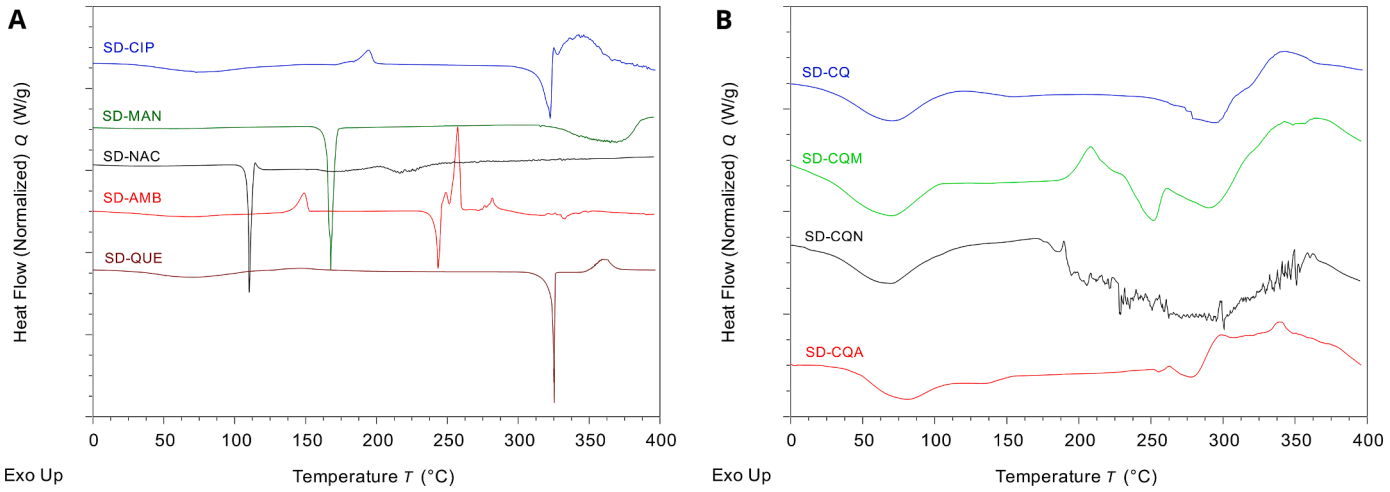

Fig. 3. DSC thermograms of (A) spray-dried single drugs and (B) spray-dried drug combinations; SD means spray-dried; CIP, QUE, MAN, NAC and AMB mean ciprofloxacin, quercetin, mannitol, N-acetylcysteine and ambroxol, respectively; CQ, CQM, CQN and CQA mean ciprofloxacin-quercetin, ciprofloxacin-quercetin-mannitol, ciprofloxacin-quercetin-N-acetylcysteine and ciprofloxacin-quercetin-ambroxol combinations, respectively.

Table 3
Thermal properties of the single and combination spray-dried drugs (mean ± SD, n = 3).

Sample	Crystallization onset (°C)	ΔH (J/g)	Melting onset (°C)	ΔH (J/g)	Tg (°C) Experimental (mDSC)	Predicted (Fox equation)
SD-CIP	182.77±1.80	52.92±0.87	315.9±1.25	226.44±15.35	86.7*	-
SD-QUE	124.25±1.48	29.31±6.01	325.04±0.53	132.66±1.23	79.51*	-
SD-MAN	-	-	166.03±0.52	283.36±4.34	12.6*	-
SD-NAC	-	-	109.73±0.13	182.28±12.65	6.9*	-
SD-AMB	141.85±0.47	49.42±0.26	241.45±0.17	138.84±8.69	87*	-
SD-CQ	-	-	-	-	148.26	84.16
SD-CQM	195.04±0.37	26.53±0.46	242.83±3.32	37.28±0.92	76.12	28.99
SD-CQN	-	-	-	-	73.45	17.75
SD-CQA	255.00±0.12	1.64±0.21	263.19±2.09	39.91±6.46	136.64	83.73

Note: SD means spray-dried; CIP, QUE, MAN, NAC and AMB mean ciprofloxacin, quercetin, mannitol, N-acetylcysteine and ambroxol, respectively; CQ, CQM, CQN and CQA mean ciprofloxacin-quercetin, ciprofloxacin-quercetin-mannitol, ciprofloxacin-quercetin-N-acetylcysteine and ciprofloxacin-quercetin-ambroxol combinations, respectively;

* experimental Tg values of amorphous CIP, QUE, MAN, NAC and AMB were taken from the literature (Lababidi et al., 2019; Mesallati et al., 2016; Sormunen et al., 2019; Tewes et al., 2013; Yu et al., 1998); experimental Tg values of spray-dried CQ, CQM, CQN and CQA were measured using mDSC.

desorption cycle. The SD-CQN powder absorbed 5.83 % (w/w) water between 0 and 80 % RH followed by a decrease in mass beyond 80 % RH which indicates a crystallization event. The desorption isotherm showed hysteresis but returned to 0 % w/w value by the end of the desorption cycle. The SD-CQA sorption isotherm showed a prominent mass increase at 80 % RH followed by a decrease in mass at 90 % RH. At the end of the desorption cycle, the SD-CQA suffers a mass loss of about 0.98 % compared to its initial mass which is most probably due to AMB hydrolysis, similar to SD-AMB, Fig. S2. (Jelić et al., 2021).

For better understanding of the events observed in DVS isotherms, the samples were also analysed by XRPD at different humidities between 0 and 90 % RH to understand the solid state changes occurring in the samples at elevated humidity (Section 3.7 XRDP).

3.4. Thermal behaviour

The thermal behaviour of spray-dried single drugs and spray-dried drug combinations are presented in Fig. 3 and Table 3.

For individually spray-dried drugs (Fig. 3A), the thermogram of SD-CIP and SD-QUE exhibited exothermic peaks at 182.77°C and 124.25°C, respectively, indicating a phase transition of amorphous CIP and QUE to crystalline forms which subsequently started melting at 315.9°C and 325.04°C, respectively (Alhajj et al., 2022). Similarly, the thermogram of SD-AMB shows a phase transition of amorphous AMB to a crystalline form with an exothermic peak onset at 141.85°C followed by a melting peak at 241.45°C and a sharp exothermic peak at 260°C due to thermal degradation (Md et al., 2021). The thermal behaviour of SD-AMB is in good agreement with the work reported by Tewes et al. (2013). The thermograms of SD-MAN and SD-NAC show no exothermic peaks but endothermic peaks at 166.03°C and 109.73°C, respectively, corresponding to their melting points (Mancini et al., 2023) indicating the crystalline nature of these materials (as confirmed by XRPD).

Fig. 3B presents the DSC thermal behaviour of the spray-dried drug combinations. The binary combination SD-CQ showed no evidence of any exothermic peaks or a sharp endothermic peak indicating the absence of any crystallization or melting events and suggesting a stable co-amorphous formulation. Among the ternary combinations, SD-CQA powder exhibited the most stable thermal behaviour without any prominent exothermic or endothermic peaks. SD-CQA shows only a very low enthalpy (ΔH = 1.64 J/g) exothermic peak onset at 255.00°C. However, SD-CQM shows prominent exothermic and endothermic peaks with onset at 195.04°C and 242.83°C, respectively, indicating crystallization and melting events. SD-CQN did not exhibit any exothermic or endothermic peaks, but it showed a degradation pattern over 170°C which is due to the degradation of NAC (Figs. S1 and S5). For better understanding of the phase transition observed by DSC, samples were subjected to XRPD at different temperatures (Section 3.7 XRDP).

Unfortunately, the DSC thermograms were not able to detect a glass

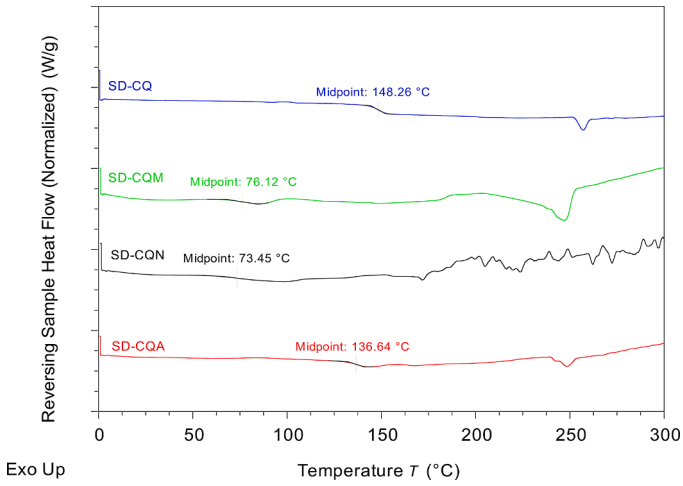

Fig. 4. mDSC thermograms (reversing heat flow) of the spray-dried combinations; SD means spray-dried; CQ, CQM, CQN and CQA mean ciprofloxacin-quercetin, ciprofloxacin-quercetin-mannitol, ciprofloxacin-quercetin-N-acetylcysteine and ciprofloxacin-quercetin-ambroxol combinations, respectively.

transition temperature (Tg) for the single drug or the ternary combination powders. For better detection and measurement of glass transitions, the samples were subjected to mDSC. However, the Tgs of the amorphous single drug powders were still not detectable. The Tgs of amorphous CIP, QUE, MAN, NAC and AMB were taken from the literature (Mesallati et al., 2016; Sormunen et al., 2019; Yu et al., 1998; Lababidi et al., 2019; Tewes et al., 2013) to calculate the predicted Tgs of the combination systems based on Fox equation (Table 3). The Tgs of the combination formulations were detectable as can be seen in the reversing heat flow signal of the mDSC thermogram (Fig. 4).

All spray-dried combinations displayed a single Tg suggesting a molecular dispersion of the respective drugs in single co-amorphous systems. For the binary combination SD-CQ, Tg was observed at 148.26°C showing a large positive deviation from the predicted Tg as calculated by Fox equation (i.e. 84.16°C) which suggests a strong molecular interaction between the CIP and QUE molecules. For the ternary combination SD-CQA, a similar positive deviation between the measured Tg (136.64°C) and the calculated Tg (83.73°C) was observed. The ternary systems SD-CQM and SD-CQN exhibited lower Tgs of 76.12°C and 73.45°C which can be attributed to the low Tg values of the mucoactive agents included in these ternary combinations (the Tg of MAN and NAC are 12.6°C and 6.9°C, respectively). Nevertheless, the measured Tgs of SD-CQM and SD-CQN are still much higher than the

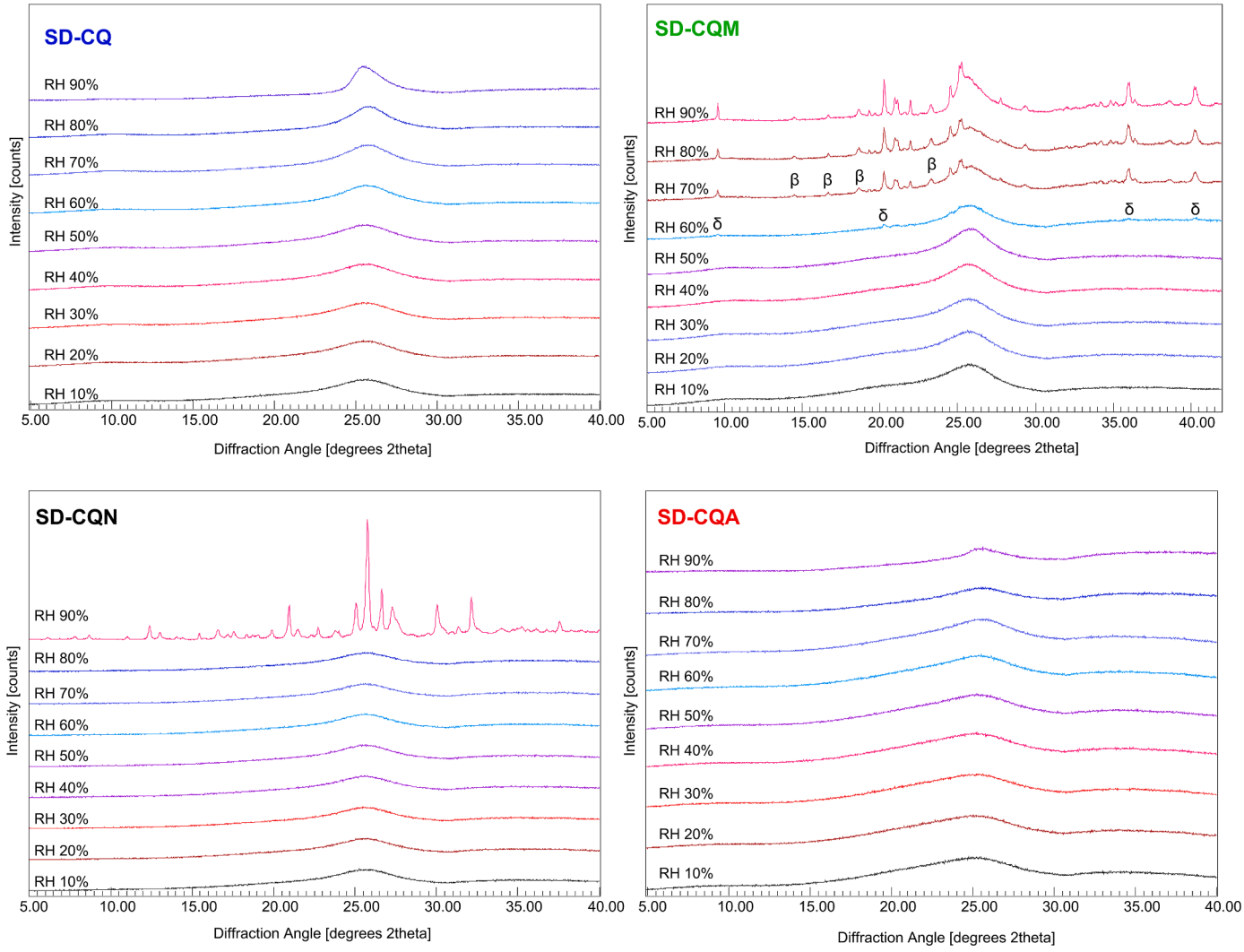

Fig. 5. X-ray diffractograms of spray-dried combinations at 25°C under different relative humidity conditions; SD means spray-dried; CQ, CQM, CQN and CQA mean ciprofloxacin-quercetin, ciprofloxacin-quercetin-mannitol, ciprofloxacin-quercetin-N-acetylcysteine and ciprofloxacin-quercetin-ambroxol combinations, respectively.

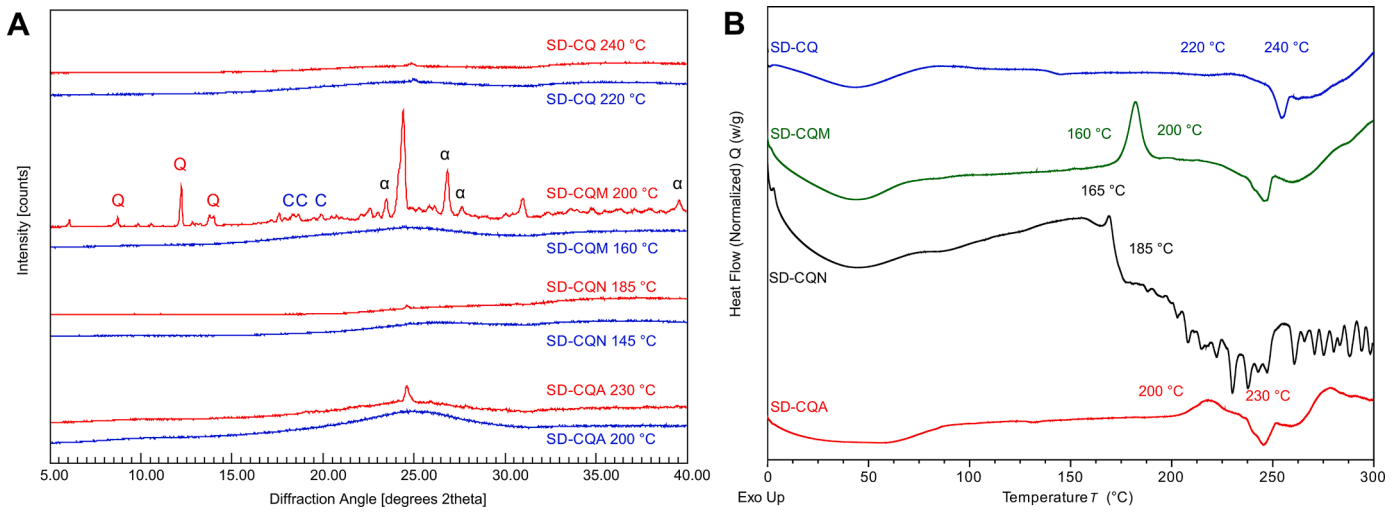

Fig. 6. A) X-ray diffractograms of the spray-dried powders under vacuum at different temperature; B) mDSC thermograms of the spray-dried powders showing the temperatures at which non-ambient XRPD was performed on each sample; SD means spray-dried; CQ, CQM, CQN and CQA mean ciprofloxacin-quercetin, ciprofloxacin-quercetin-mannitol, ciprofloxacin-quercetin-N-acetylcysteine and ciprofloxacin-quercetin-ambroxol combinations, respectively.

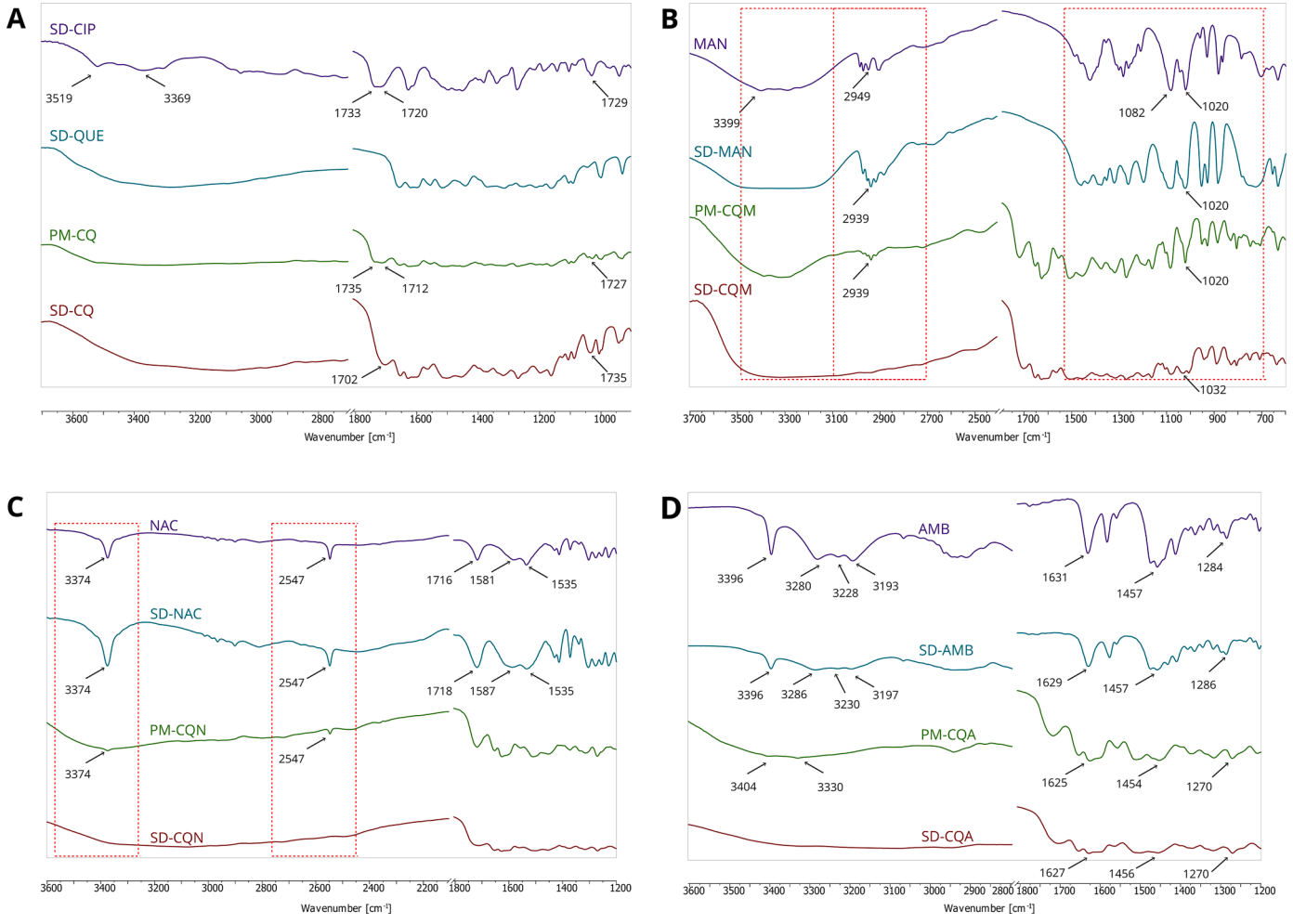

Fig. 7. FTIR spectra related to A) CQ; B) CQM; C) CQN; D) CQA; SD means spray-dried; PM means physical mixture; CIP, QUE, MAN, NAC and AMB mean ciprofloxacin, quercetin, mannitol, N-acetylcysteine and ambroxol, respectively; CQ, CQM, CQN and CQA mean ciprofloxacin-quercetin, ciprofloxacin-quercetin-mannitol, ciprofloxacin-quercetin-N-acetylcysteine and ciprofloxacin-quercetin-ambroxol combinations, respectively.

Table 4
Surface elemental composition and molar drug fraction of the spray-dried combinations.

Powder		Elemental composition (%)									Molar fraction (%)				
		C	O	Cl	N	F	S	Br	Total		CIP	QUE	MAN	NAC	AMB
SD-CQ	Theoretical	69.97	20.7	1.65	5.79	1.89	-	-	100		50.00	50.00	-	-	-
	Experimental	74.36	19.11	1.31	4.01	1.21	-	-	100		32.01	67.99	-	-	-
										Ex/Th%	64.02	135.98	-	-	-
SD-CQM	Theoretical	64.11	29.67	1.1	3.86	1.26	-	-	100		33.33	33.33	33.33	-	-
	Experimental	71.16	22.52	1.12	3.94	1.26	-	-	100		33.33	n/a	n/a	-	-
										Ex/Th%	100.00	n/a	n/a	-	-
SD-CQN	Theoretical	64.34	22.64	1.1	7.02	1.26	3.64	-	100		33.33	33.33	-	33.33	-
	Experimental	71.48	20.18	1	4.89	1.35	1.1	-	100		35.71	54.21	-	10.07	-
										Ex/Th%	107.14	162.65	-	30.21	-
SD-CQA	Theoretical	69.72	18.01	2.16	6.67	1.51	-	1.93	100		40.00	40.00	-	-	20.00
	Experimental	73.25	16.61	1.86	5.31	1.03	-	1.94	100		27.25	52.59	-	-	20.17
										Ex/Th%	68.13	131.48	-	-	100.85

Note: C, O, Cl, N, F, S and Br represent carbon, oxygen, chlorine, nitrogen, fluorine, sulphur and bromine; Ex/Th%: the ratio (%) between the experimental and theoretical molar ratios of a drug; SD means spray-dried; CIP, QUE, MAN, NAC and AMB mean ciprofloxacin, quercetin, mannitol, N-acetylcysteine and ambroxol, respectively; CQ, CQM, CQN and CQA mean ciprofloxacin-quercetin, ciprofloxacin-quercetin-mannitol, ciprofloxacin-quercetin-N-acetylcysteine and ciprofloxacin-quercetin-ambroxol combinations, respectively.

predicted values, Table 3. The calculated and measured Tgs for the ternary combinations confirm the superior thermal stability of SD-CQA over SD-CQM and SD-CQN.

3.5. Powder crystallinity by X-ray powder diffraction (XRPD)

The X-ray diffractograms of the as-received drugs and their individually spray-dried powders are presented in Fig. S3.

All as-received materials were crystalline in form as indicated by the sharp XRD Bragg peaks in their diffractograms (Fig. S3). After being spray dried individually, CIP, QUE and AMB all showed a diffuse halo, characteristic of amorphous materials, while MAN and NAC presented sharp peaks but with different patterns compared to their starting materials. The pronounced difference between as-received and spray-dried MAN is the disappearance of the peak at 23.27 2θ° and the appearance of the peak at 17.25 2θ° in spray-dried sample. The diffractograms of as-received and spray-dried MAN are in agreement with the diffractograms of β and α MAN polymorphs, respectively, as reported by Cares-Pacheco et al. (2014). Spray drying NAC resulted in the formation of a different polymorph characterized by a reduction in intensity of the peaks at 14.17 and 28.57; the disappearance of the peak at 35.05 2θ°; and the appearance of a peak at 21.22 2θ°. Aguiar et al. (2017) reported similar changes in the diffractograms of raw NAC after micronization by supercritical fluid.

Fig. S4 shows the X-ray diffractograms of the co-spray-dried combinations. All samples were in the amorphous form as indicated by the diffuse halo and the absence of any sharp peak in their respective X-ray diffractograms.

Fig. 5 presents X-ray diffractograms of the co-spray-dried combinations taken at 25°C under several relative humidity points, between 10 and 90 % RH.

Increasing the relative humidity of the samples resulted in changes in the diffractograms of two of the samples: SD-CQM and SD-CQN. SD-CQM exhibited a halo between 10 and 50 % RH. At 60 % RH, low intensity peaks started appearing on the halo at 9.57, 20.28, 35.98 and 40.29 2θ° (Fig. 5). Interestingly, these are characteristic peaks for MAN δ polymorph (Cares-Pacheco et al., 2014). At higher RH, these peaks increased in intensity and additional peaks, characteristic of the MAN β polymorph, appeared at 14.47, 16.67, 18.66 and 23.28 2θ°. This observation can explain the DVS sorption isotherm (Fig. 2) which showed a crystallization event at 60 % followed by another crystallization event at 80 % RH which is due to the formation of the MAN δ polymorph followed by the formation of the β polymorph. It should be noted that these peaks were superimposed on top of an amorphous halo and no peaks were identified for CIP or QUE. This suggests that both CIP and QUE remain in an amorphous form and only MAN crystallised. The diffractogram of SD-CQN maintained a diffuse halo between 10 and 80 % RH. At 90 % RH, the halo disappeared and several sharp peaks appeared suggesting that all three components of SD-CQN recrystallized out of the amorphous phase. By comparison, the X-ray diffractograms of formulations SD-CQ and SD-CQA remained as a diffuse halo at all RH points which indicates the stability of the amorphous state of these formulations under the experimental conditions.

The influence of temperature on the solid state properties of the spray dried combinations was investigated by taking X-ray diffractograms of the samples under vacuum at several temperature points. The temperature points were selected based on the events observed on the mDSC thermograms of each sample, which was recorded at the same heating rate i.e. 2°C/min (Fig. 6).

Fig. 6 shows that SD-CQ and SD-CQA remained amorphous when heated up to 220°C and 200°C, respectively, which is in agreement with their mDSC thermograms. Even at higher temperatures, the X-ray diffractogram maintained the halo shape with a small peak centered about 25 2θ° which suggests that the sample was still predominantly amorphous. SD-CQN maintains its amorphous state when was heated to 145°C, but it shows a degradation pattern at 185°C which can be ascribed to the degradation of NAC (Fig. S4). SD-CQM was amorphous up to 160°C and crystallized at 200°C in agreement with the mDSC thermogram. SD-CQM diffractogram shows peaks which can be assigned to CIP, QUE and the α MAN polymoph (Fig. 6). This is in contrast to the impact of elevated humidity on SD-CQM which led to the crystallization of only MAN (Fig. 5), whereas high temperature resulted in the crystallization of all three components.

3.6. Fourier transform infrared (FTIR) spectroscopy

FTIR spectra were collected for the single drugs, the spray-dried combinations i.e. SD-CQ, SD-CQM, SD-CQN and SD-CQA, and their corresponding physical mixtures of individually spray-dried drugs i.e. PM-CQ, PM-CQM, PM-CQN and PM-CQA (Fig. 7).

Fig 7A shows differences between the physical mixture and spray dried combination of CIP and QUE indicating a molecular interaction between CIP and QUE which is discussed further in the previous work (Alhajj et al., 2022).

MAN-related FTIR spectra are shown in Fig.7B. The FTIR spectra of MAN and SD-MAN are in good agreement with the reported FTIR spectra of β and α mannitol, respectively, as reported in the literature (Burger et al., 2000; Cares-Pacheco et al., 2014). This indicates that MAN underwent a transition from form β to form α during spray drying as confirmed by the XRPD data (Fig. S3). The FTIR spectrum of the ternary physical mixture PM-CQM show a pronounced peak at 2939 cm^{-1} ascribed to mannitol C-H stretching. This peak flattened and

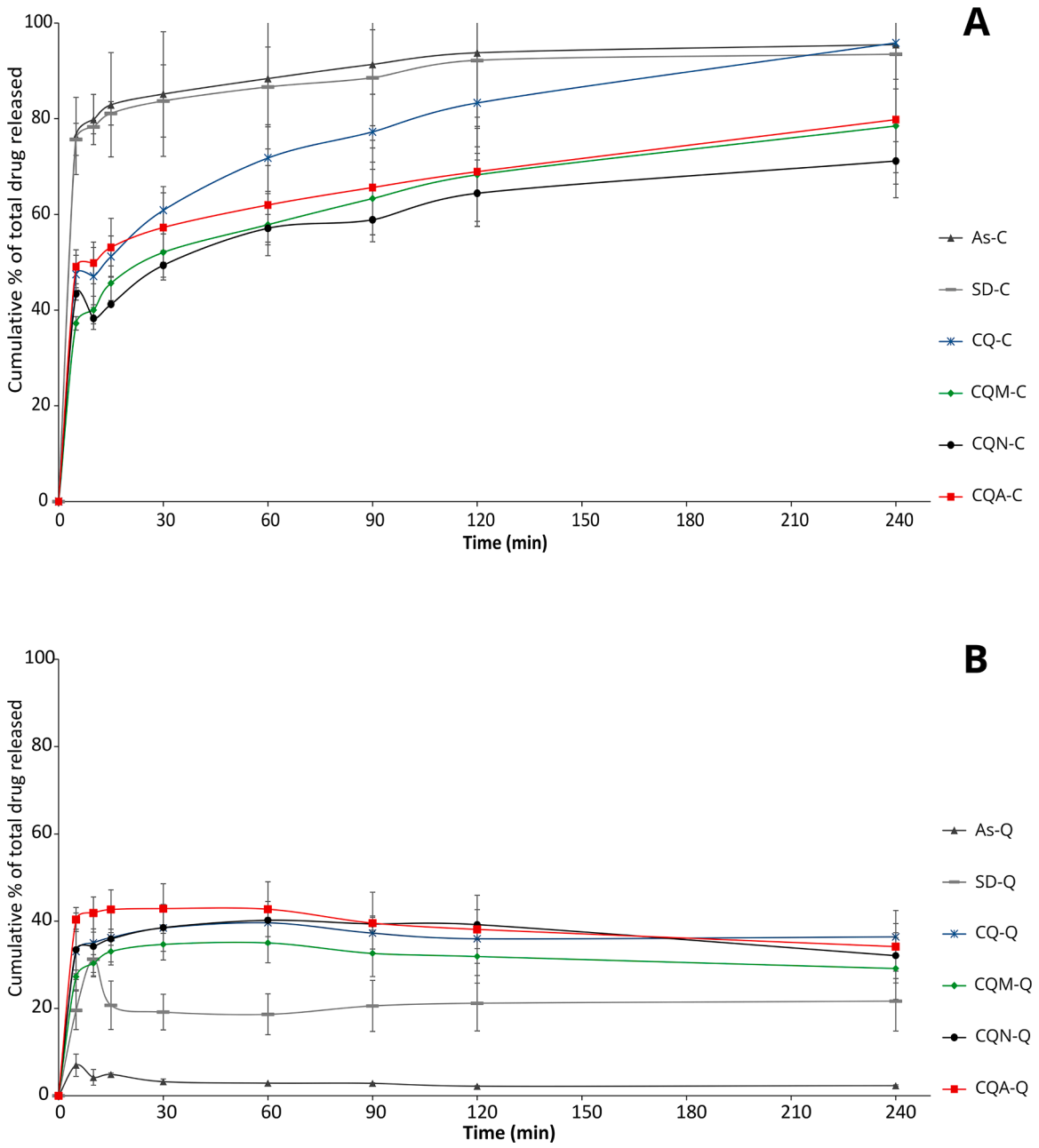

Fig. 8. *In vitro* dissolution rate profiles of A) CIP and B) QUE from their as-received (As), individually spray-dried (SD) powder and spray-dried combination powders; SD means spray-dried; CIP and QUE mean ciprofloxacin and quercetin; CQ, CQM, CQN and CQA mean ciprofloxacin-quercetin, ciprofloxacin-quercetin-mannitol, ciprofloxacin-quercetin-N-acetylcysteine, ciprofloxacin-quercetin-ambroxol combinations, respectively.

disappeared in SD-CQM spectrum. Also, the C-O stretching peaks shift from 1020 cm^{-1} in PM-COM to 1032 cm^{-1} in SD-CQM. These differences between the FTIR spectra of the physically mixed and the co-spray-dried combinations may indicate the involvement of mannitol in intermolecular interactions in the ternary co-spray-dried system.

Fig. 7C presents the FTIR spectra related to NAC. SD-NAC shows a similar FTIR spectrum with slight changes. The peaks at 1716 cm^{-1} (carboxylic group) and 1581 cm^{-1} (amide I) in NAC were broadened and reduced in intensity and shifted to 1718 cm^{-1} and 1587 cm^{-1}, respectively. These changes in the FTIR peaks might be due to the formation of a new polymorph of NAC as confirmed by XRPD (Fig. S3). The distinctive peaks of NAC at 3374 and 2547 cm^{-1} (N–H stretching bands and S–H stretching bands, respectively) can be observed in the spectrum of the physical mixture PM-CQN. However, these peaks disappeared in SD-CQN spectrum which suggests the involvement of these groups in a chemical interaction in the ternary co-amorphous system.

The FTIR spectra of AMB-related samples are presented in Fig. 7D. The AMB spectrum is in good agreement with the AMB spectrum reported by Roy et al. (2020). The peaks at 3280 cm^{-1} (N-H stretching of aromatic amine), 3228 cm^{-1} (stretching of aliphatic amine N-H) and 3193 cm^{-1} (stretching vibration of aromatic C-H) in AMB were broaden and shifted to 3286 cm^{-1}, 3230 cm^{-1} and 3197 cm^{-1} in the SD-AMB. This may be due to the transition of AMB from the crystalline to the amorphous form in SD-AMB. In the spectrum of PM-CQA physical mixture, in the region 3300–3500 cm^{-1}, several peaks of AMB, CIP and QUE overlapped and a large, broad peak can be seen. However, two low intensity peaks at 3404 cm^{-1} and 3300 cm^{-1} can be observed in this region in the PM-CQA spectrum while no peaks can be found in the spectrum of SD-CQA.

Based on the findings from the FTIR data and the positive deviation

Table 5
In vitro aerodynamic parameters of the spray dried powders (mean ± SD, n = 3).

		MMAD (μm)	GSD	ED (mg)	FPD (mg)	ED (%)	FPF (%)
SD-CIP	**CIP**	4.94 ± 0.4	2.06 ± 0.07	11.55 ± 2.65	4.41 ± 1.54	56.68 ± 5.29	21.37 ± 4.23
SD-QUE	**QUE**	3.77 ± 0.45	1.93 ± 0.04	8.49 ± 1.50	4.38 ± 0.19	44.77 ± 9.07	23.07 ± 1.68
SD-CQ	**CIP**	2.19 ± 0.01	2.05 ± 0.01	7.48 ± 0.20	6.18 ± 0.21	67.28 ± 2.92	55.64 ± 2.64
	QUE	2.32 ± 0.02	1.85 ± 0.05	5.62 ± 0.22	4.74 ± 0.17	68.28 ± 4.92	57.60 ± 3.84
SD-CQM	**CIP**	3.10 ± 0.20	2.04 ± 0.01	5.28 ± 0.43	3.61 ± 0.12	63.86 ± 1.31	43.69 ± 2.58
	QUE	3.06 ± 0.27	1.77 ± 0.01	4.18 ± 0.23	3.16 ± 0.19	63.93 ± 0.91	48.41 ± 4.18
SD-CQN	**CIP**	2.96 ± 0.16	2.46 ± 0.05	4.14 ± 0.20	2.74 ± 0.19	44.01 ± 1.84	29.07 ± 1.51
	QUE	2.98 ± 0.18	1.93 ± 0.03	2.85 ± 0.20	2.00 ± 0.18	42.09 ± 2.24	29.47 ± 1.23
SD-CQA	**CIP**	2.84 ± 0.10	2.28 ± 0.07	6.58 ± 0.42	4.54 ± 0.31	70.94 ± 3.30	48.98 ± 2.57
	QUE	2.98 ± 0.05	1.90 ± 0.02	4.39 ± 0.25	3.17 ± 0.15	70.95 ± 3.09	51.23 ± 2.78

Note: SD means spray-dried; CIP and QUE mean ciprofloxacin and quercetin; CQ, CQM, CQN and CQA mean ciprofloxacin-quercetin, ciprofloxacin-quercetin-mannitol, ciprofloxacin-quercetin-N-acetylcysteine, ciprofloxacin-quercetin-ambroxol combinations, respectively.

of the Tgs from the theoretical values, it can be assumed that molecular interactions exist between all components of the formulation in the binary and ternary co-amorphous systems. However, the strength of these interactions differ among the different co-amorphous systems as indicated by the differences in the physical stability of these systems under elevated humidity and temperature.

SD-CQ and SD-CQA exhibited the most stable amorphous states which were maintained under both elevated RH and temperature. MAN crystallised out of SD-CQM at RH values between 60 and 90 % but the system remain predominantly amorphous, while at high temperature all three components crystallised out of the SD-CQM system. In SD-CQN all three components crystallised at 90 % RH while at high temperature > 170°C NAC degraded.

3.7. Outer surface characterization by X-ray photoelectron spectroscopy (XPS)

The surface elemental composition and drug molar fraction of the spray-dried powders are presented in Table 4.

The theoretical elemental composition of the spray-dried powders was calculated based on the elemental composition of the spray-dried single drug (Table S2) by assuming that all drugs were distributed on the particle surface according to their formulation molar ratios. The experimental relative molar percentages of a drug in the top 5–10 nm layer of the spray-dried powders was calculated based on the molar percentage (derived from the XPS peak area) of its distinguishing element. The ratio (%) between the experimental and theoretical molar ratios of a drug (Ex/Th%) was calculated to compare the drug surface enrichment in different spray-dried formulations (Table 4). A value of Ex/Th% above or below 100 % suggests an over- or under-abundance of the drug on the particle surface. CIP, NAC and AMB have F, S and Br as distinguishing elements, respectively. The absence of a distinguishing element for QUE and MAN makes it impossible to calculate the QUE and MAN molar ratios in formulation SD-CQM.

In the binary formulation SD-CQ, the theoretical molar ratio of CIP and QUE is 50:50, however, XPS data shows that the top surface of SD-CQ particles were depleted of CIP and enriched with QUE (Ex/Th% = 64.02 % and 135.98 %, respectively). Since the difference between CIP and QUE molecular weights is small (331.35 g/mol vs 302.24 g/mol, respectively), this observation can be attributed to the higher hydrophobic properties of QUE compared to CIP (logP: 2.16 vs -0.86, respectively). During spray draying, ethanol evaporates faster from the water-ethanol solvent mixture due to its higher volatility and hence QUE precipitates more than CIP on the top surface of the remaining aqueous phase and the dried particles thereafter. Similarly, QUE showed a higher experimental molar ratio at the top surface of SD-CQN particles (Ex/Th % = 162.65 %). However, the addition of NAC in SD-CQN resulted in an increase in the percentage of CIP at particle surfaces compared to the binary combination SD-CQ. The Ex/Th% value of CIP increased from 64.02 % in SD-CQ to 107.14 % in SD-CQN while NAC resided preferentially below the particle surface (Ex/Th%= 30.21 %). Since CIP and NAC have similar hydrophilicity properties (logP values of -0.86 and -0.71, respectively), this observation could be due to the difference in their molecular weights. NAC has a smaller molecular weight than CIP (163.19 g/mol vs 331.346 g/mol) which results in higher diffusion rate for NAC. Therefore NAC molecules can move faster to the core of the drying droplets leaving less molecules at the surface.

Regarding SD-CQM, it is difficult to fully understand the surface composition because both QUE and MAN have no distinguishing elements. However, CIP has similar Ex/Th% values in SD-CQM and SD-CQN, 33.33 % and 35.71 %, respectively. Also, both MAN and NAC are hydrophilic molecules with small molecular weight (182.172 g/mol and 163.19 g/mol, respectively). Hence, it could be postulated that MAN has a similar impact to NAC, resulting in a similar enrichment of CIP at the particle surface.

The addition of AMB to the binary formulation had much less effect on changing the Ex/Th% values of CIP and QUE compared to NAC (Table 4). The experimental molar percentage of AMB at the surface was equal to its theoretical percentage, Ex/Th% of 100.85 %. This is could be attributed to the fact that it is equally soluble in both water and ethanol (~5 mg/ml (Ambroxol Hydrochloride | 23828-92-4, 2012)) which might result in a homogeneous distribution of AMB molecules throughout the drying droplets and within the dried particles thereafter, unlike NAC and MAN which have higher solubility in water than ethanol.

In conclusion, XPS data showed that for the binary system, QUE (a hydrophobic molecule) dominates the particle top surface at the expense of CIP (a hydrophilic molecule). The addition of a smaller second hydrophilic molecule i.e. NAC resulted in increasing the amount of CIP on the particle surface probably due to the higher diffusion rate of NAC. However, the addition of a second hydrophobic molecule which is equally soluble in both water and ethanol has a negligible impact on the distribution of CIP and QUE on the particle surface compared to their binary system.

3.8. In-vitro dissolution study

The *in vitro* dissolution profiles of CIP, QUE and their spray dried formulations were obtained in phosphate buffer solution with 0.1 % w/v tween 80 at pH 7.4 and 37°C (Fig. 8).

CIP (crystalline) and SD-CIP (amorphous) powders exhibited a similar burst release dissolution profile with about 80 % of ciprofloxacin

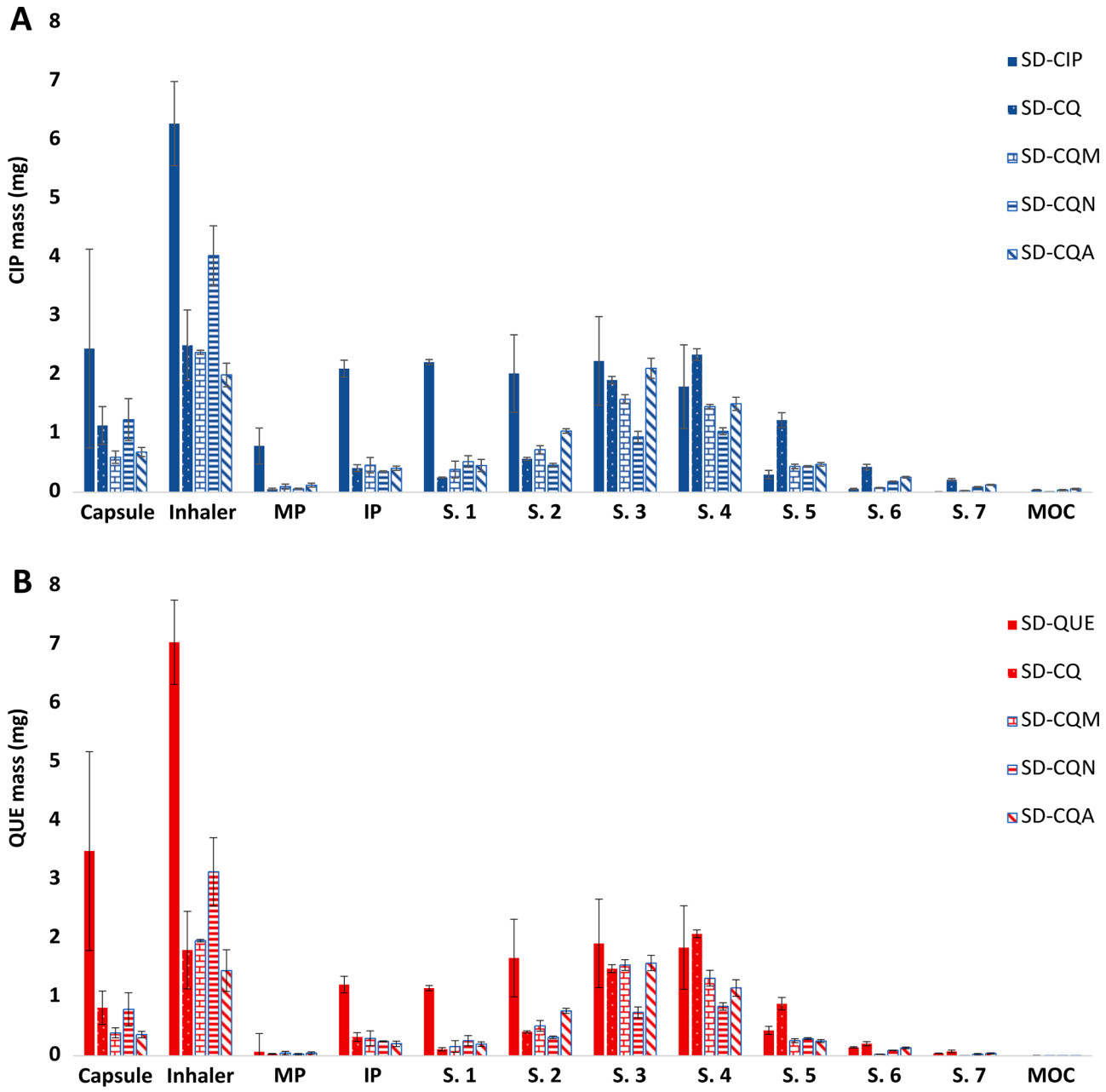

Fig. 9. The mass of (A) ciprofloxacin (B) quercetin collected from the capsule, inhaler, mouthpiece, induction port and NGI stages and filter; SD means spray-dried; CIP and QUE mean ciprofloxacin and quercetin; CQ, CQM, CQN and CQA mean ciprofloxacin-quercetin, ciprofloxacin-quercetin-mannitol, ciprofloxacin-quercetin-N-acetylcysteine, ciprofloxacin-quercetin-ambroxol combinations, respectively.

dissolved in 10 min and about 95 % dissolved by the end of the experiment (240 min). It is noteworthy that CIP is a hydrochloride monohydrate form which has higher solubility than ciprofloxacin base. The binary SD-CQ formulation released only 47 % of the ciprofloxacin in the first 10 min and 96 % by the end of the experiment. The ternary combinations showed even lower ciprofloxacin release profiles: between 40 % and 50 % ciprofloxacin was released within the first 10 min and between 70 % and 80 % was released by 240 min.

It has been found that ciprofloxacin is rapidly absorbed after pulmonary administration and pulmonary concentration of free ciprofloxacin rapidly equilibrates with the plasma free concentration (Brillault et al., 2017). Thus, the observed lower release profiles of ciprofloxacin from the combination formulations may help to prolong its *in vivo* half-life.

The as-received QUE (anhydrous quercetin) powder exhibited both the lowest extent and the slowest rate of drug dissolution. Its highest dissolved amount was 7 % reached within 5 min and then the dissolved amount decreased to 2.5 % by the end of the experiment. SD-QUE reached its highest dissolved amount of 31 % in the first 10 min followed by a sharp decrease in the next 5 min to 21 %. The value then remained at around 20 % till the end of the experiment. The reduction in the amount of dissolved quercetin could be due to the rapid recrystallization and precipitation of quercetin.

The binary and ternary systems exhibited enhanced quercetin dissolution rates compared to QUE and SD-QUE. During the first 15 min, the dissolved amounts of quercetin ranged between 33 % and 43 % for these systems, which was significantly higher than QUE i.e. 3 % ($P < 0.0001$), and SD-QUE i.e. 21 % ($P < 0.05$). However, there were no significant differences between quercetin dissolution profiles from the binary and ternary systems.

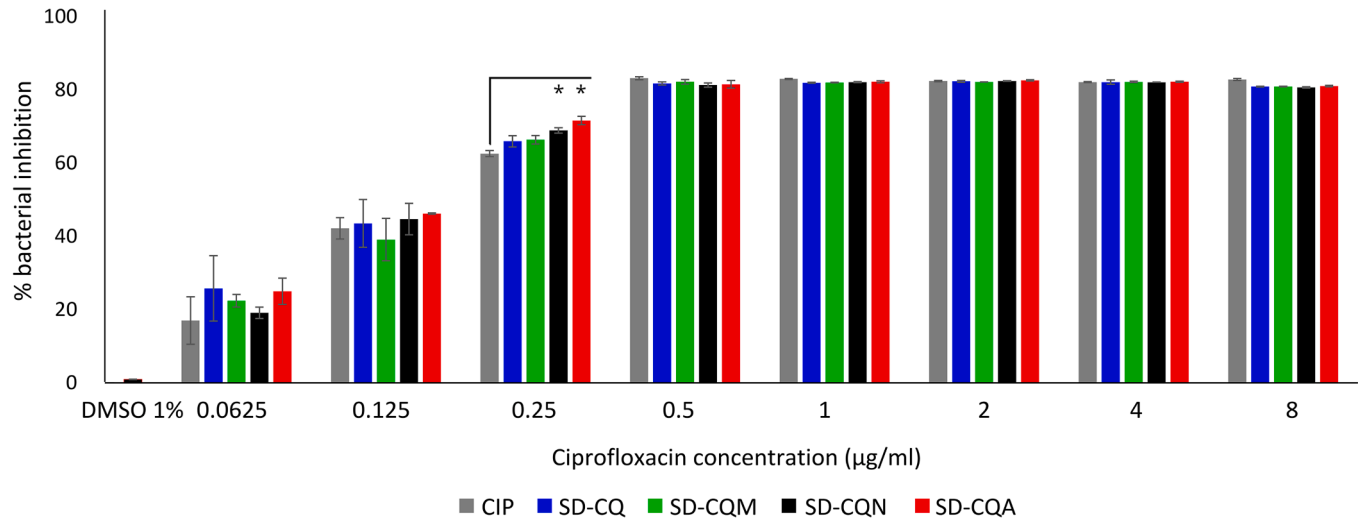

Fig. 10. Antimicrobial activity for CIP and multidrug formulations against *P. aeruginosa* ATCC 10145. * represent significant ($p < 0.05$) % bacterial inhibition potential for the multidrug formulations compared to the CIP. Means (±SD) of three triplicate; SD means spray-dried; CIP means ciprofloxacin; CQ, CQM, CQN and CQA mean ciprofloxacin-quercetin, ciprofloxacin-quercetin-mannitol, ciprofloxacin-quercetin-N-acetylcysteine and ciprofloxacin-quercetin-ambroxol combinations, respectively.

These results indicate that the presence of quercetin (a poorly-water soluble drug) and a drug with a higher water solubility i.e. ciprofloxacin in a co-amorphous system was effective in improving the solubility of quercetin. This might be attributed to the higher water-solubility of the ciprofloxacin molecules which changes the microenvironment of the dissolution surface of the co-amorphous solid bringing more dissolution media into contact with quercetin molecules. A similar effect was reported by Lee et al. (2014) whereby ciprofloxacin was found to improve the water solubility of beclomethasone dipropionate from a drug-drug co-amorphous formulation.

3.9. Powder flow properties and cohesion

The low bulk density of SD-CIP and SD-QUE compared to the co-spray dried powder can be explained by differences in their particle sizes and shapes. SD-CIP and SD-QUE exhibited large particle sizes and irregular shapes respectively, while co-spray drying the two drugs together resulted in small spherical particles and hence increased bulk density (Changmai and Purkait, 2021; Ridgway and Rupp, 1969). Carr's index was between 36.7 % (SD-CQA) and 57.1 % (SD-CIP). Carr's index shows a positive correlation with particle cohesion measured by the shear cell apparatus (Pearson correlation = 0.90; $p = 0.016$).

In spite of having larger particle size, SD-CIP exhibited the highest cohesion value ($p < 0.05$). Interestingly, a positive correlation was found to exist between the molar percentage of CIP on the particle surface of the spray-dried combinations, measured by XPS (Table 4), and particle cohesiveness (Table 2) (Pearson correlation = 0.90; $p = 0.04$) which confirms the role of the co-spray dried material in reducing the particle cohesion by reducing the percentage of hygroscopic CIP at the particle surface.

3.10. Aerosolization performance

The aerosolization parameters of the spray dried powders were calculated for both CIP and QUE, and are presented in Table 5.

It is noteworthy that the loaded powder mass for the *in vitro* aerosolization test in this study is 20 mg which is double the amount used in our previous study (Alhajj et al., 2022). For SD-CQ, increasing the loaded powder from 10 mg to 20 mg reduced the ED% from 86.93 % and 80.24 % to 56.68 % and 44.77 %, for CIP and QUE respectively. However, the FPDs from the 20 mg SD-CQ were 6.18 mg and 4.74 mg, for CIP and QUE respectively, which is much higher than previously achieved from the 10 mg i.e. 2.67 mg and 2.32 mg, respectively.

Considering the ternary combinations, SD-CQA achieved the highest ED% which could be due to its comparatively low Carr's index and cohesion values (Table 2) which resulted in better flowability and dispersion. SD-CQN exhibited the lowest ED% among all spray-dried combinations ($p < 0.01$) which could be for several reasons. Firstly, SD-CQN has a comparatively high Carr's index and cohesion values compared to the other ternary combinations. However, SD-CQN exhibited a lower ED% than SD-CQ although the Carr's index and cohesion values of SD-CQ are not different from SD-CQN. It seems that the presence of NAC on the surface of SD-CQN particles increased the powder adhesion on the capsule and the inhaler device as seen in Fig. 9.

For the combination formulations, the mass ratios between ciprofloxacin and quercetin in the recovered powder from the cascade and their mass ratios in the powder collected from stages 1–5 were in good agreement with the nominal mass ratios. This indicates that no substantial segregation occurred during storage, handling, aerosolization and deposition of the powders.

3.11. In vitro antibacterial activities against P. aeruginosa

To investigate whether the addition of quercetin and/or the mucoactive agents modulate the antibacterial activity of as-received CIP against *P. aeruginosa*, the minimum inhibitory concentration (MIC) of CIP and the spray-dried combinations was determined against *P. aeruginosa* (ATCC 10145) using the broth microdilution method. The MIC of CIP was found to be 0.5 µg/ml which is in the EUCAST breakpoints (European Committee on Antimicrobial Susceptibility Testing [EUCAST], 2022) for CIP against *P. aeruginosa* and in good agreement with the MIC of CIP against *P. aeruginosa* (ATCC 10145) obtained by Arauzo et al. (2021). The MIC of all spray-dried combinations were similar to CIP i.e. 0.5 µg/ml, Fig. S6.

In addition, the bacterial inhibition potential of the spray dried combinations was measured by comparing serial dilutions of the spray-dried combinations versus as-received CIP (Fig. 10).

At concentrations ≥ 1 MIC (i.e. 0.5 µg/ml), the antibacterial effect of all spray-dried combinations showed no difference compared to CIP; all samples induced > 80 % bacterial inhibition growth.

Thus, the antimicrobial effect of CIP was not comprised but was conserved or enhanced in the spray-dried combinations.

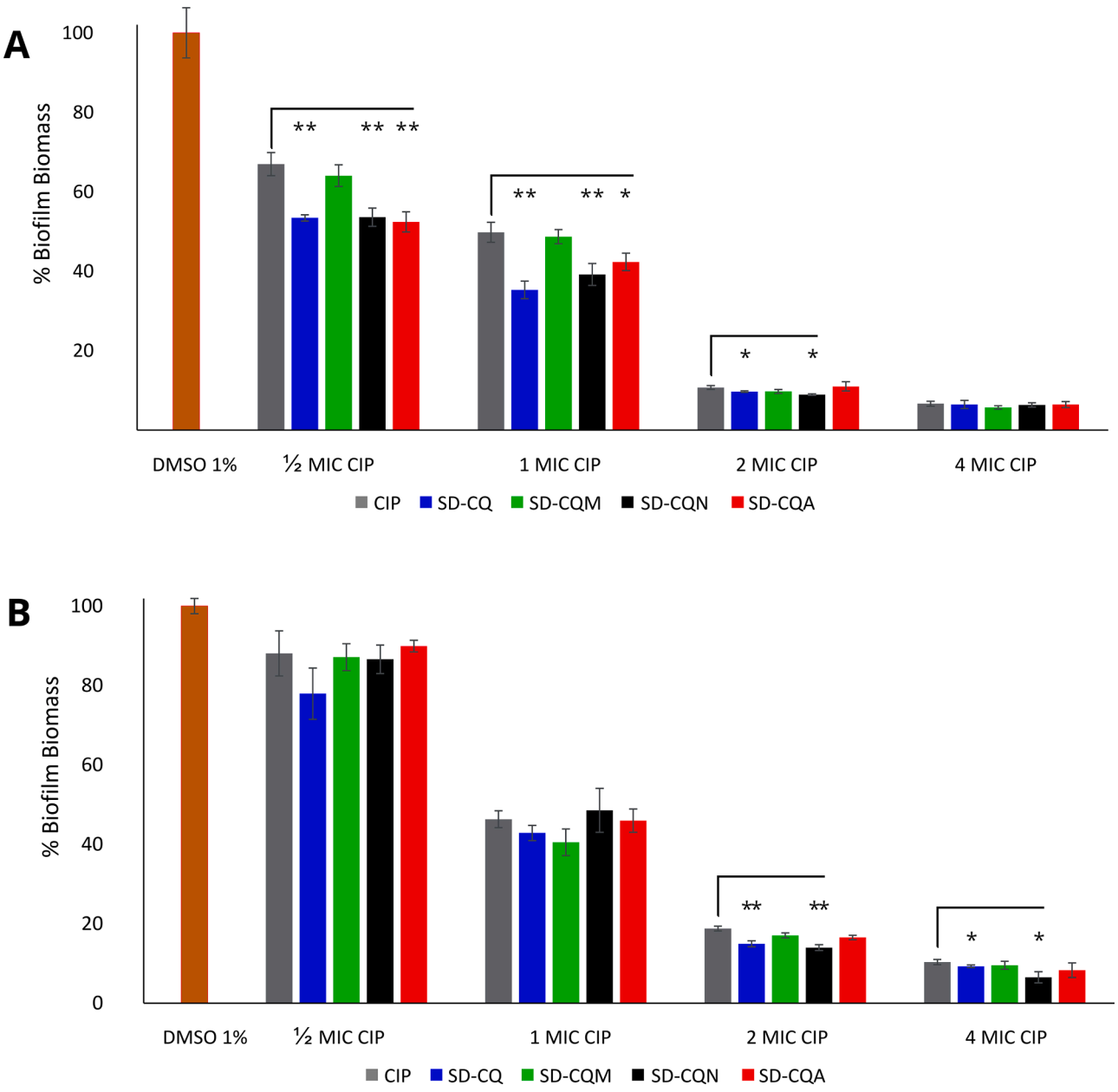

Fig. 11. A) Inhibition of biofilm formation and B) Disruption of pre-established biofilm (48-h old) of *P. aeruginosa* ATCC 10145. Testes were performed at various concentrations of CIP and multidrug dry powder formulation formulations. * and ** represent significant ($p < 0.05$ and $p < 0.01$, respectively) decreases of biofilm biomass for the multidrug formulations compared to the CIP. Means (±SD) of three triplicate; SD means spray-dried; CIP means ciprofloxacin; CQ, CQM, CQN and CQA mean ciprofloxacin-quercetin, ciprofloxacin-quercetin-mannitol, ciprofloxacin-quercetin-N-acetylcysteine and ciprofloxacin-quercetin-ambroxol combinations, respectively.

3.12. In vitro evaluation of the effect of spray-dried combinations on P. aeruginosa biofilm formation inhibition and biofilm disaggregation

Inhibiting biofilm formation is a highly sought after goal because antibiotic therapies against established biofilm infections is not usually effective (Khan et al., 2021). The effects of as-received CIP and the spray-dried combinations on inhibiting biofilm formation and disrupting a pre-established biofilm were evaluated by crystal violet (CV) biofilm assay (Fig. 11).

All samples were screened at different antibiotic concentrations (½ MIC, 1 MIC, 2 MIC and 4 MIC) to reveal the effect of the spray-dried combination on biofilm at the appropriate concentration because the potential effect can be concealed by the inhibition of bacterial growth at high antibiotic concentration.

In regard to biofilm inhibition, CIP and the spray-dried combinations exhibited significant reduction in biofilm biomass at all concentrations compared to the negative control i.e. DMSO 1 % ($p < 0.0001$) (Fig. 11A).

QUE has proven strong anti-biofilm effects on *P. aeruginosa* (Memariani et al., 2019). Previous work showed that QUE at concentration of 8 μg/ml resulted on 36 % reduction *P. aeruginosa* biofilm production (Ouyang et al., 2016). Aghavi et al. investigated the effect of QUE and CIP combination on inhibiting *P. aeruginosa* biofilm formation. They found that even at low concentrations as 1/16 MIC of both QUE and CIP, the combination exhibited significant biomass reduction compared to the single drug (Taghavi et al., 2021). In the present study, the binary formulation SD-CQ and the ternary formulations SD-CQN and SD-CQA exhibited much reduction in the biofilm biomass compared to CIP at ½ MIC and 1 MIC (Fig. 11A) while at higher concentration there was no

significant difference between CIP and the spray-dried combinations which could be due to the high concentration of the antibiotic in these formulations.

The effect of SD-CQM in inhibiting biofilm formation was no different from the as-received CIP. This is could be due to the presence of mannitol in this formulation. Žiemytė et al. (2021) found that high concentration of MAN can enhance the antibacterial activity of subinhibitory concentrations of CIP against *P. aeruginosa* but MAN at low concentration can be metabolised by the bacteria and consequently the bacteria start to initiate biofilm formation again. Hence, one possibility is that the presence of MAN in SD-CQM compromised the effect of QUE against biofilm formation.

The antibiofilm effects of the spray-dried combinations and CIP were further test on a 48h pre-established biofilm (Fig. 11B). It can be seen that at ½ MIC all samples had less efficacy against pre-established biofilm than inhibiting biofilm formation. At 1 MIC, 2 MIC and 4 MIC, CIP and the spray-dried combinations exhibited significant reduction in pre-established biofilm biomass compared to the negative control i.e. 1 % DMSO ($p < 0.0001$) (Fig. 11B). Compared to CIP, only formulations SD-CQ and SD-CQN at 2 MIC and 4 MIC showed statically significant difference in disrupting the biofilm but the difference is very low (<5 %) which seems insignificant practically.

A critical factor in the antibiotic treatment against bacterial infection is the relationship between the concentration of the antibiotic and its minimum inhibitory concentration against the target bacteria. Ciprofloxacin, like other fluoroquinolones, is a concentration-dependent antibiotic and hence its effectiveness depends on the extent to which the ciprofloxacin concentration is above the MIC. In order to achieve successful clinical and microbiological treatment, and to avoid the development of bacterial resistance, ciprofloxacin needs to be delivered at a concentration of at least 10-fold above the MIC (Wright et al., 2000). There is no optimal method for determining the volume of human epithelial lung fluid (ELF) and the values reported in the literature are between 20 and 40 ml (Fröhlich et al., 2016). Table 5 shows that the FPD of CIP from the spray-dried combinations ranges between 6.18 mg and 2.74 mg which would result in CIP concentration in ELF (40 ml) between 154.50 μg/ml and 68.50 μg/ml which is 309 and 137 time its MIC. SD-CQA, a promising formulation with favourable physical stability properties, would result in CIP concentration of 227-fold greater than the MIC.

Considering the physical instability and poor aerosol performance of SD-CQM and SD-CQN, both formulations should be excluded from any future work for testing their mucoactivity. Ambroxol showed promising results which should be investigated further. However, given that ambroxol exerts its pharmacologyical effect via stimulating the mucociliary clearance, stimulating surfactant secretion and increasing cough effectiveness via its mucokinetic properties (Scaglione and Petrini, 2019) SD-CQA would require *in vivo* testing using animal model, which is beyond the scope of our work at this time.

4. Conclusion

Inhaled formulations of CIP, QUE and three different mucoactive agents were prepared and characterised. Of these it was found that of SD-CQM and SD-CQN showed physical instability manifesting as phase transitions the amorphous state under elevated humidity and/or temperature. Both formulations also showed inferior *in vitro* aerosol performance compared to SD-CQA. By comparison, the SD-CQA combination was amorphous and showed physical stability under both elevated humidity and temperature as indicated by DVS, DSC and XRPD. Furthermore, SD-CQA was highly respirable (ED ~ 70 %) with an *in vitro* ciprofloxacin fine particle dose that would exceed the MIC in the epithelial lung fluid by > 200-fold. SD-CQA exhibited *in vitro* antibacterial and antibiofilm activity against *P. aeruginosa* (ATCC 10145). The *in vitro* dissolution profile of SD-CQA displayed slower dissolution of ciprofloxacin and enhanced dissolution of quercetin compared to the single drugs. Overall, SD-CQA has a promising potential role in the treatment of *P. aeruginosa* lung infections in CF. SD-CQA deserves further research investigating the optimum molar ratio that maintains the physical stability and yields best aerosol performance, pharmacokinetic and pharmacodynamic profile using an *in vivo* infected animal model.

CRediT authorship contribution statement

Nasser Alhajj: Conceptualization, Methodology, Data curation, Validation, Formal analysis, Investigation, Writing – original draft. **Mohd Fakharul Zaman Raja Yahya:** Validation, Writing – review & editing, Supervision. **Niall J. O'Reilly:** Conceptualization, Validation, Resources, Writing – review & editing, Supervision. **Helen Cathcart:** Conceptualization, Validation, Resources, Writing – review & editing, Supervision.

Declaration of Competing Interest

The authors declare that they have no known competing financial interests or personal relationships that could have appeared to influence the work reported in this paper.

Data availability

Data will be made available on request.

Acknowledgment

The research conducted in this publication was funded by The Irish Research Council under award number [GOIPG/2021/26] and the South East Technological University (SETU) PhD Scholarship Programme (Nasser Al-hajj); funding from The Higher Education Authority (HEA)—COVID-19 costed extension by the Department of Further and Higher Education is gratefully acknowledged.

Supplementary materials

Supplementary material associated with this article can be found, in the online version, at doi:10.1016/j.ejps.2023.106654.

References

Aguiar, G.P.S., Marcon, M., Mocelin, R., Herrmann, A.P., Chaves, L.M.P.C., Piato, A.L., Lanza, M., Oliveira, J.V., 2017. Micronization of N-acetylcysteine by supercritical fluid: evaluation of *in vitro* and *in vivo* biological activity. J. Supercrit. Fluids 130, 282–291. https://doi.org/10.1016/j.supflu.2017.06.010.

Ahmed, M.N., Abdelsamad, A., Wassermann, T., Porse, A., Becker, J., Sommer, M.O.A., Høiby, N., Ciofu, O., 2020. The evolutionary trajectories of *P. aeruginosa* in biofilm and planktonic growth modes exposed to ciprofloxacin: beyond selection of antibiotic resistance. npj Biofilms Microbiomes 6, 28. https://doi.org/10.1038/s41522-020-00138-8.

Alhajj, N., O'Reilly, N.J., Cathcart, H., 2023. Quality by design – spray drying of ciprofloxacin-quercetin fixed-dose combination intended for inhalation. Int. J. Pharm. 642, 123151 https://doi.org/10.1016/j.ijpharm.2023.123151.

Alhajj, N., O'Reilly, N.J., Cathcart, H., 2022. Development and characterization of a spray-dried inhalable ciprofloxacin-quercetin co-amorphous system. Int. J. Pharm. 618, 121657 https://doi.org/10.1016/j.ijpharm.2022.121657.

Alhajj, N., O'Reilly, N.J., Cathcart, H., 2021. Developing ciprofloxacin dry powder for inhalation: a story of challenges and rational design in the treatment of cystic fibrosis lung infection. Int. J. Pharm. 613, 121388 https://doi.org/10.1016/j.ijpharm.2021.121388.

Ambroxol Hydrochloride | 23828-92-4, 2012. Sax's Dangerous Properties of Industrial Materials. https://doi.org/10.1002/0471701343.sdp26898.

Arauzo, B., Lobera, M.P., Monzon, A., Santamaria, J., 2021. Dry powder formulation for pulmonary infections: ciprofloxacin loaded in chitosan sub-micron particles generated by electrospray. Carbohydr. Polym. 273, 118543 https://doi.org/10.1016/j.carbpol.2021.118543.

Asano, J., Niisato, N., Nakajima, K.I., Miyazaki, H., Yasuda, M., Iwasaki, Y., Hama, T., Dejima, K., Hisa, Y., Marunaka, Y., 2009. Quercetin stimulates Na+/K+/2Cl-

cotransport via PTK-dependent mechanisms in human airway epithelium. Am. J. Respir. Cell Mol. Biol. 41, 688–695. https://doi.org/10.1165/rcmb.2008-0338OC.
Bernardy, E.E., Petit 3rd, R.A., Raghuram, V., Alexander, A.M., Read, T.D., Goldberg, J. B., 2020. Genotypic and phenotypic diversity of staphylococcus aureus isolates from cystic fibrosis patient lung infections and their interactions with *Pseudomonas aeruginosa*. mBio 11. https://doi.org/10.1128/mBio.00735-20 e00735-20.
Bhagwat, S., Schilling, U., Chen, M.J., Wei, X., Delvadia, R., Absar, M., Saluja, B., Hochhaus, G., 2017. Predicting pulmonary pharmacokinetics from *in vitro* properties of dry powder inhalers. Pharm. Res. 34, 2541–2556. https://doi.org/10.1007/s11095-017-2235-y.
Brillault, J., Tewes, F., Couet, W., Olivier, J.C., 2017. *In vitro* biopharmaceutical evaluation of ciprofloxacin/metal cation complexes for pulmonary administration. Eur. J. Pharm. Sci. 97, 92–98. https://doi.org/10.1016/j.ejps.2016.11.011.
Brunaugh, A.D., Sharma, S., Smyth, H., 2021. Inhaled fixed-dose combination powders for the treatment of respiratory infections. Expert Opin. Drug Deliv. 18, 1101–1115. https://doi.org/10.1080/17425247.2021.1886074.
Burger, A., Henck, J.O., Hetz, S., Rollinger, J.M., Weissnicht, A.A., Stöttner, H., 2000. Energy/temperature diagram and compression behavior of the polymorphs of D-mannitol. J. Pharm. Sci. 89, 457–468.
Cares-Pacheco, M.G., Vaca-Medina, G., Calvet, R., Espitalier, F., Letourneau, J., Rouilly, A., Rodier, E., 2014. Physicochemical characterization of D-mannitol polymorphs: the challenging surface energy determination by inverse gas chromatography in the infinite dilution region. Int. J. Pharm. 475, 69–81.
Chang, R.Y.K., Das, T., Manos, J., Kutter, E., Morales, S., Chan, H.K., 2019. Bacteriophage PEV20 and ciprofloxacin combination treatment enhances removal of *Pseudomonas aeruginosa* biofilm isolated from cystic fibrosis and wound patients. AAPS J. 21, 49. https://doi.org/10.1208/s12248-019-0315-0.
Changmai, M., Purkait, M.K., 2021. Chapter 10 - membrane adsorption. T. (Ed.). Adsorption: Fundamental Processes and Applications. Elsevier, pp. 629–653. https://doi.org/10.1016/B978-0-12-818805-7.00007-2.
de Castro, R.R., Todaro, V., da Silva, L.C.R.P., Simon, A., do Carmo, F.A., de Sousa, V.P., Rodrigues, C.R., Sarmento, B., Healy, A.M., Cabral, L.M., 2020. Development of inhaled formulation of modified clofazimine as an alternative to treatment of tuberculosis: clofazimine inhaled formulation for tuberculosis. J. Drug Deliv. Sci. Technol. 58 https://doi.org/10.1016/j.jddst.2020.101805.
Eedara, B.B., Bastola, R., Das, S.C., 2022. Dissolution and absorption of inhaled drug particles in the lungs. Pharmaceutics 14, 2667.
European Committee on Antimicrobial Susceptibility Testing (EUCAST), 2022. EUCAST: Clinical breakpoints and dosing of antibiotics [WWW Document]. Eur. Comm. Antimicrob. Susceptibility Test. URL https://www.eucast.org/clinical_breakpoints (accessed 11.30.23).
Fröhlich, E., Mercuri, A., Wu, S., Salar-Behzadi, S., 2016. Measurements of deposition, lung surface area and lung fluid for simulation of inhaled compounds. Front. Pharmacol. 7, 181.
Henke, M.O., Ratjen, F., 2007. Mucolytics in cystic fibrosis. Paediatr. Respir. Rev. 8, 24–29. https://doi.org/10.1016/j.prrv.2007.02.009.
Hill, D.B., Long, R.F., Kissner, W.J., Atieh, E., Garbarine, I.C., Markovetz, M.R., Fontana, N.C., Christy, M., Habibpour, M., Tarran, R., 2018. Pathological mucus and impaired mucus clearance in cystic fibrosis patients result from increased concentration, not altered pH. Eur. Respir. J. 52.
Jelić, D., Papović, S., Vraneš, M., Gadžurić, S., Berto, S., Alladio, E., Gajić, D., Janković, B., 2021. Thermo-analytical and compatibility study with mechanistic explanation of degradation kinetics of ambroxol hydrochloride tablets under non-isothermal conditions. Pharmaceutics 13, 1910.
Karagianni, A., Kachrimanis, K., Nikolakakis, I., 2018. Co-amorphous solid dispersions for solubility and absorption improvement of drugs: composition, preparation, characterization and formulations for oral delivery. Pharmaceutics 10, 98.
Khan, J., Tarar, S.M., Gul, I., Nawaz, U., Arshad, M., 2021. Challenges of antibiotic resistance biofilms and potential combating strategies: a review. 3 Biotech 11, 1–15.
Lababidi, N., Montefusco-Pereira, C.V., de Souza Carvalho-Wodarz, C., Lehr, C.M., Schneider, M., 2020. Spray-dried multidrug particles for pulmonary co-delivery of antibiotics with N-acetylcysteine and curcumin-loaded PLGA-nanoparticles. Eur. J. Pharm. Biopharm. 157, 200–210. https://doi.org/10.1016/j.ejpb.2020.10.010.
Lababidi, N., Ofosu Kissi, E., Elgaher, W.A.M., Sigal, V., Haupenthal, J., Schwarz, B.C., Hirsch, A.K.H., Rades, T., Schneider, M., 2019. Spray-drying of inhalable, multifunctional formulations for the treatment of biofilms formed in cystic fibrosis. J. Control. Release 314, 62–71. https://doi.org/10.1016/j.jconrel.2019.10.038.
Lee, S.H., Teo, J., Heng, D., Zhao, Y., Ng, W.K., Chan, H.K., Tan, R.B.H., 2014. Steroid-decorated antibiotic microparticles for inhaled anti-infective therapy. J. Pharm. Sci. 103, 1115–1125. https://doi.org/10.1002/jps.23874.
Liao, C., Huang, X., Wang, Q., Yao, D., Lu, W., 2022. Virulence factors of *Pseudomonas aeruginosa* and antivirulence strategies to combat its drug resistance. Front. Cell. Infect. Microbiol. 12.
Mancini, L., Paolantoni, M., Schoubben, A., Ricci, M., 2023. Development of spray-dried N-acetylcysteine dry powder for inhalation. Int. J. Pharm. 631, 122550 https://doi.org/10.1016/j.ijpharm.2022.122550.
Mancuso, G., Midiri, A., Gerace, E., Biondo, C., 2021. Bacterial antibiotic resistance: the most critical pathogens. Pathogens. https://doi.org/10.3390/pathogens10101310.
Mangal, S., Huang, J., Shetty, N., Park, H., Lin, Y., Yu, H.H., Zemlyanov, D., Velkov, T., Li, J., Zhou, Q.T., 2019a. Effects of the antibiotic component on in-vitro bacterial killing, physico-chemical properties, aerosolization and dissolution of a ternary-combinational inhalation powder formulation of antibiotics for pan-drug resistant Gram-negative lung infections. Int. J. Pharm. 561, 102–113. https://doi.org/10.1016/j.ijpharm.2019.02.018.
Mangal, S., Park, H., Nour, R., Shetty, N., Cavallaro, A., Zemlyanov, D., Thalberg, K., Puri, V., Nicholas, M., Narang, A.S., Zhou, Q.T., 2019b. Correlations between surface composition and aerosolization of jet-milled dry powder inhaler formulations with pharmaceutical lubricants. Int. J. Pharm. 568, 118504 https://doi.org/10.1016/j.ijpharm.2019.118504.
Md, S., Abdullah, S.T., Alhakamy, N.A., Bani-Jaber, A., Radhakrishnan, A.K., Karim, S., Shahzad, N., Gabr, G.A., Alamoudi, A.J., Rizg, W.Y., 2021. Ambroxol hydrochloride loaded gastro-retentive nanosuspension gels potentiate anticancer activity in lung cancer (A549) cells. Gels. https://doi.org/10.3390/gels7040243.
Memariani, H., Memariani, M., Ghasemian, A., 2019. An overview on anti-biofilm properties of quercetin against bacterial pathogens. World J. Microbiol. Biotechnol. 35, 143. https://doi.org/10.1007/s11274-019-2719-5.
Merritt, J.H., Kadouri, D.E., O'Toole, G.A., 2011. Growing and analyzing static biofilms. Curr. Protoc. Microbiol. 22, 1B–11.
Mesallati, H., Mugheirbi, N.A., Tajber, L., 2016. Two faces of ciprofloxacin: investigation of proton transfer in solid state transformations. Cryst. Growth Des. 16, 6574–6585. https://doi.org/10.1021/acs.cgd.6b01283.
Ouyang, J., Sun, F., Feng, W., Sun, Y., Qiu, X., Xiong, L., Liu, Y., Chen, Y., 2016. Quercetin is an effective inhibitor of quorum sensing, biofilm formation and virulence factors in *Pseudomonas aeruginosa*. J. Appl. Microbiol. 120, 966–974. https://doi.org/10.1111/jam.13073.
Paczkowski, J.E., Mukherjee, S., McCready, A.R., Cong, J.P., Aquino, C.J., Kim, H., Henke, B.R., Smith, C.D., Bassler, B.L., 2017. Flavonoids suppress *Pseudomonas aeruginosa* virulence through allosteric inhibition of quorum-sensing receptors. J. Biol. Chem. 292, 4064–4076. https://doi.org/10.1074/jbc.M116.770552.
Qin, S., Xiao, W., Zhou, C., Pu, Q., Deng, X., Lan, L., Liang, H., Song, X., Wu, M., 2022. *Pseudomonas aeruginosa*: pathogenesis, virulence factors, antibiotic resistance, interaction with host, technology advances and emerging therapeutics. Signal Transduct. Target. Ther. 7, 199. https://doi.org/10.1038/s41392-022-01056-1.
Ratjen, F., Wönne, R., Posselt, H.G., Stöver, B., Hofmann, D., Bender, S.W., 1985. A double-blind placebo controlled trial with oral ambroxol and N-acetylcysteine for mucolytic treatment in cystic fibrosis. Eur. J. Pediatr. 144, 374–378. https://doi.org/10.1007/BF00441781.
Ridgway, K., Rupp, R., 1969. The effect of particle shape on powder properties. J. Pharm. Pharmacol. 21, 30S–39S.
Roy, N., Bomzan, P., Nath Roy, M., 2020. Probing host-guest inclusion complexes of ambroxol hydrochloride with α- & β-cyclodextrins by physicochemical contrivance subsequently optimized by molecular modeling simulations. Chem. Phys. Lett. 748, 137372 https://doi.org/10.1016/j.cplett.2020.137372.
Scaglione, F., Petrini, O., 2019. Mucoactive agents in the therapy of upper respiratory airways infections: fair to describe them just as mucoactive? Clin. Med. Insights. Ear Nose Throat 12, 1179550618821930.
Son, Y.J., Horng, M., Copley, M., McConville, J.T., 2010. Optimization of an *in vitro* dissolution test method for inhalation formulations. Dissolut. Technol. 17, 6–13.
Sormunen, H., Ruponen, M., Laitinen, R., 2019. The effect of co-amorphization of glibenclamide on its dissolution properties and permeability through an MDCKII-MDR1 cell layer. Int. J. Pharm. 570, 118653 https://doi.org/10.1016/j.ijpharm.2019.118653.
Srichana, T., Martin, G.P., Marriott, C., 1998. Dry powder inhalers: the influence of device resistance and powder formulation on drug and lactose deposition *in vitro*. Eur. J. Pharm. Sci. 7, 73–80. https://doi.org/10.1016/S0928-0987(98)00008-6.
Taghavi, T., Zeighami, H., Heidari, A., Gholami, M., Rafiee, F., Haghi, F.. Anti-quorum sensing activity of quercetin in combination with imipenem and ciprofloxacin against Pseudomonas aeruginosa PAO1. https://doi.org/10.21203/rs.3.rs-435536/v1.
Tarrant, B.J., Maitre, C.L., Romero, L., Steward, R., Button, B.M., Thompson, B.R., Holland, A.E., 2019. Mucoactive agents for adults with acute lung conditions: a systematic review. Hear. Lung 48, 141–147. https://doi.org/10.1016/j.hrtlng.2018.09.010.
Tewes, F., Paluch, K.J., Tajber, L., Gulati, K., Kalantri, D., Ehrhardt, C., Healy, A.M., 2013. Steroid/mucokinetic hybrid nanoporous microparticles for pulmonary drug delivery. Eur. J. Pharm. Biopharm. 85, 604–613. https://doi.org/10.1016/j.ejpb.2013.03.020.
Thai, T., Salisbury, B.H., Zito, P.M., 2021. Ciprofloxacin, in: StatPearls. StatPearls Publishing.
Varelogianni, G., Hussain, R., Strid, H., Oliynyk, I., Roomans, G.M., Johannesson, M., 2013. The effect of ambroxol on chloride transport, CFTR and ENaC in cystic fibrosis airway epithelial cells. Cell Biol. Int. 37, 1149–1156. https://doi.org/10.1002/cbin.10146.
Vasavi, H.S., Arun, A.B., Rekha, P.D., 2016. Anti-quorum sensing activity of flavonoid-rich fraction from Centella asiatica L. against *Pseudomonas aeruginosa* PAO1. J. Microbiol. Immunol. Infect. 49, 8–15. https://doi.org/10.1016/j.jmii.2014.03.012.
Vipin, C., Mujeeburahiman, M., Ashwini, P., Arun, A.B., Rekha, P.D., 2019. Anti-biofilm and cytoprotective activities of quercetin against *Pseudomonas aeruginosa* isolates. Lett. Appl. Microbiol. 68, 464–471. https://doi.org/10.1111/lam.13129.
Wang, S., Yao, J., Zhou, B., Yang, J., Chaudry, M.T., Wang, M., Xiao, F., Li, Y., Yin, W., 2018. Bacteriostatic effect of quercetin as an antibiotic alternative *in vivo* and its antibacterial mechanism *in vitro*. J. Food Prot. 81, 68–78. https://doi.org/10.4315/0362-028X.JFP-17-214.
Wayne, P.A., 2010. Clinical and Laboratory Standards Institute: Performance standards for antimicrobial susceptibility testing: 20th informational supplement. CLSI Doc M100-S20.
Wright, D.H., Brown, G.H., Peterson, M.L., Rotschafer, J.C., 2000. Application of fluoroquinolone pharmacodynamics. J. Antimicrob. Chemother. 46, 669–683.

Yu, L., Mishra, D.S., Rigsbee, D.R., 1998. Determination of the glass properties of D-mannitol using sorbitol as an impurity. J. Pharm. Sci. 87, 774–777.

Zhang, S., Smith, N., Schuster, D., Azbell, C., Sorscher, E.J., Rowe, S.M., Woodworth, B. A., 2011. Quercetin increases cystic fibrosis transmembrane conductance regulator-mediated chloride transport and ciliary beat frequency: therapeutic implications for chronic rhinosinusitis. Am. J. Rhinol. Allergy 25, 307–312. https://doi.org/10.2500/ajra.2011.25.3643.

Žiemytė, M., Carda-Diéguez, M., Rodríguez-Díaz, J.C., Ventero, M.P., Mira, A., Ferrer, M. D., 2021. Real-time monitoring of *Pseudomonas aeruginosa* biofilm growth dynamics and persister cells' eradication. Emerg. Microbes Infect. 10, 2062–2075. https://doi.org/10.1080/22221751.2021.1994355.